CONCURRENT DESIGN AND PROCESS OPTIMIZATION IN FORGING

by

Sinem Kocaoğlan

B.S., Mechanical Engineering, Celal Bayar University, 2008

Submitted to the Institute for Graduate Studies in
Science and Engineering in partial fulfillment of
the requirements for the degree of
Master of Science

Graduate Program in Mechanical Engineering

Boğaziçi University

2013

ACKNOWLEDGEMENTS

I would like to express my gratitude to my thesis supervisor Prof. Fazıl Önder Sönmez for introducing me to the field of finite elements and his valuable guidance and helpfulness throughout this study.

I would like to thank Murat Öztürk for his aid and hard work on optimization of forging process. Also I would like to thank Niyazi Tanlak for his great helps during computational progress and encouragements.

Lastly, I would like to thank to my family and Alper Mert for their endless understanding and support.

ABSTRACT

CONCURRENT DESIGN AND PROCESS OPTIMIZATION IN FORGING

Design parameters not only affect the performance of a product, but also affect the feasibility, effectiveness and efficiency of manufacturing. Processing parameters, in turn, affect the performance of the part. For this reason, a design optimization study focusing on just design parameters may result in a design difficulty to manufacture or a processing optimization study considering just processing parameters may result in a product with inferior quality. Therefore, effective optimization of a product requires a joint consideration of all these variables. In this study, a concurrent design optimization methodology is proposed to minimize the cost of a cold forging process using both product design and process design parameters as optimization variables. An objective function is defined combining material cost, manufacturing cost, and post manufacturing (shearing) cost of the product. The part to be optimized is a simply supported I-beam under a centric load. Because of large number optimization variables, a two-level approach is adopted. In the first level, only design variables defining the geometry of the part are considered to optimize its shape. In the second one, all of the process variables like preform dimensions and fillet radii and some of the design variables are considered. Various constraints are imposed related to the performance of the product in working condition and the effectiveness of manufacturing. Nelder-Mead, a robust zero - order search algorithm, is used as the search algorithm and analyses are carried out using commercial finite element software, ANSYS. After repeated runs, results are obtained that show considerable improvement in the cost.

ÖZET

DÖVME İŞLEMİNDE EŞZAMANLI TASARIM VE PROSES OPTİMİZASYONU

Tasarım parametreleri sadece ürün performansını değil, aynı zamanda üretimin uygulanabilirliliğini, geçerliliğini ve verimliliğini etkiliyor. Dolayısıyla, proses parametreleri parça performansını da etkiliyor. Bu nedenle, sadece tasarım parametrelerine odaklanmış bir tasarım optimizasyonu üretimi zor olan bir tasarım ile sonuçlanabilir veya sadece işlem parametrelerini dikkate alan proses optimizasyon çalışması düşük kaliteli ürün ile sonuçlanabilir. Bu nedenle, bir ürünün optimizasyonu için hepsinin birleşimi olan değişkenlere ihtiyaç duyulur. Bu çalışmada, eşzamanlı tasarım optimizasyon metodu hem ürün hem de proses tasarım parametreleri optimizasyon değişkenleri olarak kullanılarak soğuk dövme işleminin maliyetini en aza indirgemek için önerilmektedir. Objektif fonksiyon malzeme maliyeti, üretim amliyeti ve ürünün imalat sonrası (kesme) maliyeti birleştirilerek tanımlandı. Optimize edilen parça merkezi bir yük altındaki basit mesnetli I-profildir. Çok sayıdaki optimizasyon değişkenleri nedeniyle iki aşamalı yaklaşım benimsenmiştir. Birinci aşamada, sadece parçanın geometrisini tanımlayan tasarım değişkenleri şekli optimize etmek için dikkate alındı. İkinci aşamada ise, kalıp boyutları, kavis yarıçapları ve tasarım değişkenleri gibi tüm proses değişkenleri dikkate alındı. Çalışma koşullarındaki ürün perfomansına ve üretim verimliğine ilişkin çeşitli kısıtlamalar düzenlendi. Sıfırıncı dereceden dayanıklı bir algoritma olan Nelder-Mead arama algoritması kullanıldı ve analizler ticari sonlu elemanlar yazılımı olan ANSYS kullanılarak yapıldı. Tekrarlanan döngüler sonucunda maliyette dikkate değer gelişmeler olduğunu gösteren sonuçlar elde edildi.

TABLE OF CONTENTS

ACKNOWLEDGEMENTS iii
ABSTRACT iv
ÖZET v
LIST OF FIGURES viii
LIST OF TABLES x
LIST OF SYMBOLS xi
1. INTRODUCTION 1
2. PROBLEM STATEMENT 6
3. OPTIMIZATION METHODOLOGY 8
3.1. Design Variables 8
3.2. Formulation of the Objective Function 10
3.2.1. Material Cost, c_m 11
3.2.2. Forging Cost, c_f 11
3.2.3. Shearing Cost, c_s 12
3.3. Constraints and Penalty Functions 13
3.4. Optimization Procedure 15
3.4.1. First Level Optimization 16
3.4.2. Second Level Optimization 17
3.5. Search Algorithm 18
3.6. Finite Element Modeling 22
3.6.1. First Level Model 22
3.6.2. Second Level Model 24
3.7. Structural Analysis 30
3.7.1. Yield Strength after Forging 30
3.7.2. Residual Stress Calculations 32
3.7.3. Failure Analysis of the I-Beam during Its Use 34
3.7.4. Lateral Buckling 36
3.8. Convergence Analysis 38
3.8.1. Convergence Analysis of First Level 39

3.8.2. Convergence Analysis of Second Level 40
4. RESULTS AND DISCUSSIONS 43
4.1. First Level Optimization Results 43
4.2. Second Level Optimization Results 44
5. SUMMARY AND CONCLUSIONS 48
APPENDIX A: NELDER MEAD ALGORITHM 50
APPENDIX B: FLOW CURVE DATA USED IN MISO MODEL 54
APPENDIX C: VOLUME OF DIE CAVITY 55
APPENDIX D: LATERAL BUCKLING 56
APPENDIX E: MAXIMUM DISTORTION ENERGY THEORY 58
REFERENCES 61

LIST OF FIGURES

Figure 2.1. A schema of simply supported I-beam under centric load [54]. 6

Figure 2.2. Manufacturing phases of the I-beam [53, 54]. 7

Figure 3.1. Cross-sectional shape of the I-beam. 9

Figure 3.2. Dimensions of quarter part of the I-beam processed by forging [54]. 10

Figure 3.3. Flow chart of the optimization process. 21

Figure 3.4. SOLID95 with its 20 nodes [65]. 23

Figure 3.5. Meshed I-beam [65]. 23

Figure 3.6. Boundary conditions applied on the I-beam [65]. 24

Figure 3.7. FE Model in Ansys. 25

Figure 3.8. PLANE183 with its 8 nodes [65]. 25

Figure 3.9. Meshed FE model with contact pairs and boundary conditions. 26

Figure 3.10 Finite element results of I-beam for same geometric parameters with different friction coefficients. 28

Figure 3.11. MISO flow curve of SAE 1010 generated in ANSYS [65]. 30

Figure 3.12. Expected failure locations in the I-beam. 31

Figure 3.13. Von Mises Stress distribution after loading. 32

Figure 3.14. Residual stresses in the z direction after unloading. 33

Figure 3.15. Loading condition [56]. 34

Figure 3.16. Von misses stress distribution of the part including cavity. 38

Figure 3.17. Part at the middle stage of the process. 41

Figure 3.18. Last view of animation. 41

Figure 4.1. The final shape of the optimum part. 46

Figure 4.2. Von Mises Stress in the optimum part. 47

Figure 4.3. Equivalent plastic strain in the optimum part. 47

Figure A.1. Triangle *BGW* and point ***R*** and extended point ***E*** [8]. 51

Figure A.2. The contraction point C_1 or C_2 for Nelder-Mead method [8]. 52

Figure A.3. Shrinking the triangle toward ***B*** [8]. 52

LIST OF TABLES

Table 3.1. The relations between the geometric parameters and their values. 9

Table 3.2. The upper and lower limits (in mm) on the variables in the first level. 17

Table 3.3. The upper and lower limits (in mm) on the parameters in the second level. 18

Table 3.4. Maximum von Misses stresses corresponding to different element sizes. 39

Table 3.5. Maximum von Misses stresses corresponding to different refinement sizes. 39

Table 3.6. Maximum Von Misses stresses and strains corresponding to different element sizes. 40

Table 4.1. Results of the first level optimization. 44

Table 4.2. Results of the second level optimization. 45

Table 4.3. Energy and stress values for optimum part. 46

Table A.1. Logical decisions for the Nelder-Mead algorithm [8]. 50

Table B.1. Flow curve data used in MISO model. 54

LIST OF SYMBOLS

b	Width
B	Best point of the Nelder-Mead Triangle
c	Distance between the neutral axis and the furthermost point
c	Penalty coefficient
c_f	Forging cost
c_m	Material cost
c_s	Shearing cost
c_{11}	Constant used for shearing
c_{22}	Constant used for shearing
C_1	Contradiction point of the Nelder-Mead Triangle
C_2	Contradiction point of the Nelder-Mead Triangle
E	Expansion point of the Nelder-Mead Triangle
E	Modulus of elasticity
f	Total cost function
F	Force applied
F_{cr}	Critical load of lateral buckling
F_l	Flash length
G	Shear modulus of elasticity
G	Good point of the Nelder-Mead Triangle
h	Flange width without web thickness
h_f	Height
h_w	Height of the web
H	Half of the preform height
I_w	Torsion warping constant
I_{yy}	Moment of inertia of the I-beam with respect to the y-axis
I_{zz}	Moment of inertia of the I-beam with respect to the z-axis

J	Torsion constant
ℓ	Flash Volume
L	Half of the preform width
L_b	Beam length
L_o	Half height of web including radii
L_1	Half of web height
L_2	Half height of I-beam
M	Middle point of the Nelder-Mead Triangle
$M_{\max}$	Maximum bending moment
p_e	Local electricity price for industry
p_m	Unit price of the material
P	Penalty function
$P_{\max}$	Maximum contact pressure on the punch
Q	First moment with respect to neutral axis of the cross section
r_1	Radius between flange and web of the I-beam
r_2	Radius of flange
r_3	Radius of flange
r_4	Radius of flange
R	Reflection point of the Nelder-Mead Triangle
s	Stroke
S	Shrinking point of the Nelder-Mead Triangle
S_{ut}	Tensile strength of the material
S_y	Yield strength of the material
t	Thickness
t_b	Half burr thickness
t_f	Thickness of the flange
t_w	Thickness of the web
U_f	Total strain energy of deformation of the final part

U_s	Shearing energy
V	Volume of material
V	Shearing force
V_d	Volume of the die cavity
V_p	Volume of the part
w	Flange thickness without radii
W	Worst point of the Nelder-Mead Triangle
x	Optimization variable
x_ℓ	Lower bound
x_u	Upper bound

α_1	Draft angles
α_2	Draft angles
ε_T	True strain
$\dot{\varepsilon}_{ij}$	Total (elastic and plastic) strain rates
η_f	Efficiency with which electricity converted to deformation energy
η_s	Efficiency of the shearing operation
ρ	Density of the material
σ_{all}	Allowable compressive stress of the mold material
σ_{eq}	Equivalent stress
σ_E	Engineering stress
σ_{ij}	Components of the stress tensor
$\sigma_{\max}$	Maximum equivalent stress
σ_T	True stress
τ	Shearing stress
τ_{allow}	Allowable shearing stress

1. INTRODUCTION

Various manufacturing methods can be used to produce mechanical parts. A suitable method is chosen based on the geometry of the part, the required quality, the quantity to be produced, and the manufacturing cost. In this study, forging, which is one of the widely used manufacturing methods for metals, is considered. If the forming process occurs below the recrystallization temperature of the metal, the process is named ‘cold forging’. This has certain advantages such as high dimensional accuracy, superior mechanical properties and microstructure. Furthermore forging to net or near-net shape dimensions reduces material cost as well as post processing cost. However, because of the relatively high tooling and equipment costs, the process is feasible only if the part is to be produced in large quantities [1].

In the traditional approach, manufacturing procedure is decided based on experience. In most cases, values for processing parameters selected based on experience and intuition do not give satisfactory results. Thus, they are modified according to outputs of a trial-and-error-correction phase. For manufacturing processes requiring high tooling costs, these trial-and-error efforts drastically decrease the efficiency of the product development endeavors. Besides, the resulting processing conditions would be less than the optimum. The traditional approach has become obsolete through the developments in the computer technology. Numerical methods like FEM allow prediction of the effects of process parameters on the end product by simulating the manufacturing process. This reduces trial-and-error efforts dramatically. On the other hand, FEM as an analysis tool only provides outputs for a predetermined process; it cannot appraise these outputs and suggest a better process design. Integration of simulation models with optimization algorithms helps to determine optimum processing conditions. The forging process has a number of parameters that are under the control of the process designer, which can be used to optimize the process. By optimizing the controllable process parameters, one can improve the product quality and manufacturing efficiency, and decrease costs significantly. In a process optimization study, according to the desired optimization aim, a suitable objective function is constructed. Choosing the objective and constraint functions, the optimization variables, and search algorithm has paramount importance on the effectiveness of the optimization. In the literature, different approaches were adopted in this respect.

In the previous studies of forging process optimization, the researchers considered forging of cylinders produced by upsetting [2-13], H-shaped axisymmetric parts [5, 14-25], two-ribbed blocks [26], aerofoil blades [3, 27, 28, 29, 30], axisymmetric parts [2, 8, 31-36], some 2D parts [10, 37, 38], 3D complex-shaped parts [39], steering links [40], wheels [30, 37], hubs [41, 42], spindles [43], and gears [25, 43]. In some of these studies [2, 4, 14, 26, 27], forging process was simulated to take place as hot, in others [5, 9, 10, 16, 17, 18, 21, 25, 28, 31, 32, 39, 41, 43] as cold. In an optimization procedure, depending on the quality and cost requirements on the part, a suitable objective function is chosen. In the previous studies, the goal was to minimize either the forming energy [2, 4, 5, 12, 19, 33, 43, 44], total strain energy [5, 20, 24, 37], total energy [4, 5, 13, 14, 35], average elasto-plastic strain [20], tendency for tensile fracture [34], cost [45], excess material or flash, which is the portion of the workpiece bulging out of the die, to obtain net shape [15, 30, 39, 41, 46], variation in hardness distribution [6], grain size [21, 37], effective strain variation [17, 22, 24, 35, 36, 37, 42], force applied by the tools [39, 42, 43], forging errors in the component [3, 14, 27 ,29] difference between realized and desired final forging shapes [7-10, 12, 23, 28, 44], material use [11], initial die temperature [18] or ram velocity [18], the difference between maximum and minimum effective plastic strains in the final product [32], total deformation energy [32] and strain variance [40] or die fatigue life was maximized [31]. Besides, multi-objective optimization problems were considered where the objective was to minimize the difference between the realized and prescribed final forged shape and total energy [12, 47]. In some cold forging operations, deformation becomes so extensive that forging operations are conducted in sub-steps followed by annealing. Hence, in some studies [4, 5, 15, 18, 43, 25], the number of forming stages was optimized. In forging process optimization studies, optimization variables are chosen among the processing parameters that have significant effect on the objective function. Parameters defining die approach angles, the area reduction ratio and the number of passes or drafts [32], die shape [15, 16, 25, 30, 33, 34, 38, 48], preform shape [6, 9, 25, 30], number of forming operations [34], thickness of the flash [20], temperature [4, 18], velocity [18, 21, 43], friction coefficient [33, 49], load paths [49], distance between boundary points [44 ,48], force applied by the tools [33, 35], height [43, 46], fillet radii [6, 11, 20, 46], preform dimensions[21, 43, 46] were selected optimization variables in the optimization problems considered in the previous studies. Because the computational time required for simulations of metal forming processes is generally very high, only the most effective parameters should be chosen. In a process optimization procedure, while improving the objective function by modifying the optimization parameters, constraints are imposed on these parameters to avoid underfilling of the die cavity [5, 14, 18, 19, 21, 30, 35, 36, 39-43 46], difference between the produced shape and the target shape [3, 4, 7-11, 13, 14, 17, 23, 34, 37], shape errors [10], excessive flash [21, 41], structural failure of die [48] or to ensure dimensional accuracy [5, 16, 49], and to limit areas of die [16], effective stress[30], effective strain rate [19, 30, 41], and to limit temperature [4, 13, 14] and load [22].

In most applications, the manufacturing efficiency, manufacturability, cost, and the quality of the resulting product depend on both processing and design parameters. For this reason, integrating product design and manufacturing design phases, which is called concurrent design approach, enables selection of more appropriate values for these parameters. Accordingly, designing forged products includes not only the optimization of the part geometry and material but also the selection of appropriate manufacturing process conditions so that desired properties can be obtained (strength, tolerances, residual stresses, grain structure, surface properties, etc.) with minimum cost. Through the use of an optimization algorithm with the concurrent design procedure, both manufacturing process and part performance can be optimized. A concurrent design optimization scheme includes both design and processing parameters as optimization variables and also design and manufacturing constraints. Some concurrent design optimization procedures were previously developed by several researchers [26, 45, 50, 51] for several manufacturing processes. Chang and Bryant [50] minimized the cost of aircraft torque tubes, piston and cylinder components and the tube weight by using the part thicknesses as optimization variables. Virtual prototyping and rapid prototyping were employed to support both product and process re-engineering in a concurrent manner. The design and the processing were optimized concurrently to minimize 10-40 % of the volume but maintain its strength. Al-Ansaray and Deiab [51] minimized the total machining cost of mechanical assemblies including the cost of all individual machining operations by taking product design dimensional tolerances and machining tolerances as optimization variables. They considered two mechanical systems, piston-cylinder assembly and rotor assembly, and optimized the tolerances of their individual parts. Janakiraman *et al.* [45] minimized total manufacturing cost and quality loss cost which is the loss of money due to a deviation away from targeted performance as a function of measured response. Three cost components; operation cost, tool cost and tool replacement cost are included in the objective function. Number of rough turning passes used and cutting speed, feed and depth of cut in each step are taken as optimization parameters and depth of cut, tolerence of process, upper and lower limits were set on machining parameters, cutting force, power and surface roughness are used as constraints. Chen and Simon [52] optimized product performance and welding process. Height of the beam, thickness of the beam, depth of the weld and length of the weld [52] were selected as the optimization variables in the optimization problem. Constraints on these parameters are imposed to avoid deflection, bending stress and buckling load [52].

In this thesis, the goal is to develop a concurrent design optimization methodology to minimize the overall cost of forged products by using product design parameters as well as processing design parameters as optimization variables. Because of their large number, a multilevel approach is adopted. In the first level, the material cost is minimized using the dimensional parameters, i.e. only design variables, as optimization variables. Side constraints on the height, width and thickness of the I-beam, are imposed as constraints. In the second level, processing parameters and also some of the design parameters are used to minimize the overall cost which includes the material cost, manufacturing cost and post-manufacturing cost. Design constraints regarding failure of the part during its use as well as manufacturing constraints are imposed.

After Öztürk’s thesis [53], this is the first study on concurrent design optimization of forging processes. There is only one study using a concurrent approach in forging process optimization [26]; however it is rather on the development of a support software module aimed at assisting manufacturing design decisions. This system combined theoretical and empirical knowledge about a variety of aspects of product design and manufacturing, and thus, it provided reasoning and decision-making capability for engineers in a way to decide on some factors like material type, lubricant, or machine type. In comparison to the forging optimization studies that considered a part with similar geometry like the references [20], a larger number of parameters are considered as optimization variables and also a larger number of constraints.

2. PROBLEM STATEMENT

The aim of this study is to develop a concurrent design optimization methodology that can solve the combined optimization problem of product design and processing design phases. A cold forging process was chosen as the manufacturing process to be optimized.

The part to be optimized is a beam with an I-cross section simply supported and subjected to a centric load as the worst loading condition during its use as shown in Figure 2.1. Beams with I-cross-sections are generally used in the industry due to their good load carrying capacity under bending.

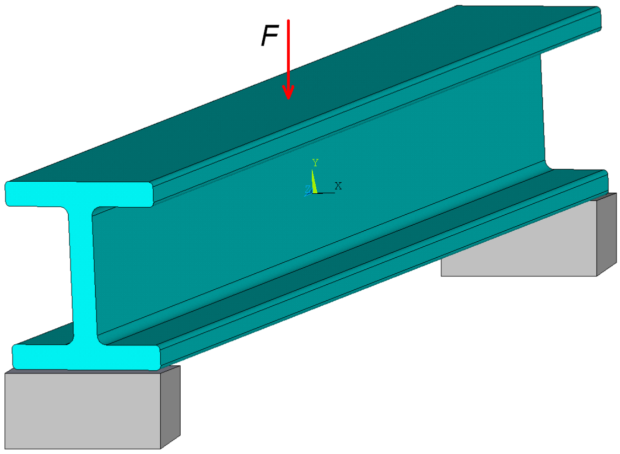

Figure 2.1. A schema of simply supported I-beam under centric load [54].

Manufacturing of an I-beam can be achieved either by forging or extrusion. The choice between extrusion and forging is made based on manufacturing cost, mechanical properties desired and the length of the beam. The part considered in this study is manufactured through forging followed by a shearing operation. As illustrated in Figure 2.2, first the rectangular bar is forged into I-beam cross-section and this operation is followed by the shearing of the flashes.

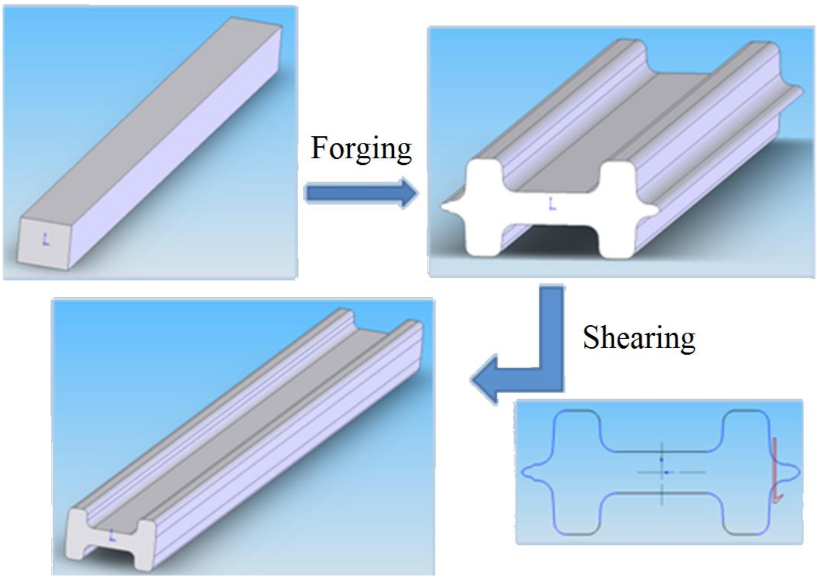

Figure 2.2. Manufacturing phases of the I-beam [53, 54].

The objective is to find the optimum values of the design and processing variables that minimize the total cost including the material cost and the manufacturing cost. The optimization is subject to both behavioral and manufacturing constraints. The behavioral constraints include failure conditions due to static yielding and local buckling during the use of the beam. Satisfaction of these constraints ensures safe use of the part. The manufacturing constraints include die filling, the maximum allowable pressure on the die and limited flash out of the die. In this way, the billet fills up the die, no damage is done to the dies during forging, and the length of the flashes, i.e. material waste, is minimized. Both manufacturing and design parameters are chosen as optimization variables. Design variables are the dimensions of the I-beam; manufacturing variables are the fillet radii, thickness of the flash and preform dimensions.

3. OPTIMIZATION METHODOLOGY

A typical design optimization problem is solved through the following stages: Formulation of the objective function to be minimized; selection of the design variables affecting the value of the objective function and the constraint functions; setting the constraints; defining penalty function, weight coefficients; selection of the search algorithm.

3.1. Design Variables

Effectiveness of the optimization procedure depends on the proper choice of the optimization variables. All the parameters having appreciable effect on the objective function or the constraint functions should be chosen as optimization variables. On the other hand, the parameters having insignificant effect should be taken as constant.

Figure 3.1 shows the cross-section of the I-beam and the geometric parameters defining the section. Because I-beams are doubly symmetric, one of the representative quarters is used in the analysis as depicted in Figure 3.2. Forging is achieved by forcing the upper die to move a certain distance, *s*. The stroke, *s*, depends on the height of the preform, 2*H*, and the thickness of the web. The parameters chosen as optimization variables are the thickness of the flange, t_f, thickness of the web, t_w, width, *b*, height of the web, h_w, fillet radii, r_1, r_2, r_3, and r_4, half of the preform dimensions, *H* and *L*, and half burr thickness, t_b. These variables include the design parameters as well as the processing parameters. The design parameters are the dimensions of the cross section, t_f, t_w, h_f, *b*; these mainly affect the performance of the part. The processing parameters are the preform dimensions, *H* and *L*, the fillet radii, and the burr thickness, t_b; these mainly influence the effectiveness of manufacturing. Length of the preform, *L*, is not directly taken as a variable; instead the volume of the die cavity, V_d, is calculated and *L* is expressed as

$$L = V_d / H + \ell \tag{3.1}$$

where ℓ is taken as an optimization variable. The draft angles of the flange, α_1 and α_2, are taken as constant and equal to 3° as in the study of Khoury *et al.* [20]. Table 3.1 gives the relations between the geometric parameters of design optimization and processing optimization and also the values of the parameters taken constant.

Table 3.1. The relations between the geometric parameters and their values.

Width	$b = 2(H + h - s)$
Height	$h_f = 2(L_o + w - r_3)$
Flange Thickness	$t_f = w + r_2 + r_3$
Web Thickness	$t_w = 2(H - s)$
Web Height	$h_w = h_f - 2t_f$
Draft angles	$\alpha_1, \alpha_2 = 3^{\circ}$
Beam length	$L_b = 200mm$
Half of web height	$L_1 = L_o - r_1 - r_2 - (h - r_1 - r_2).tan\,\alpha_1$

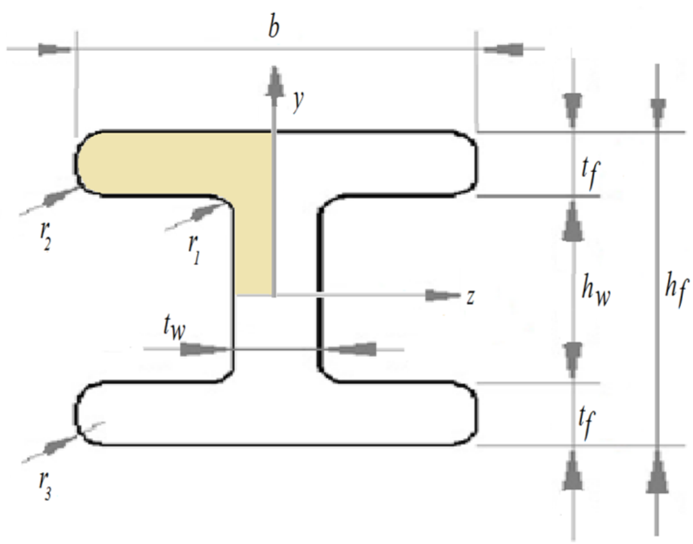

Figure 3.1. Cross-sectional shape of the I-beam.

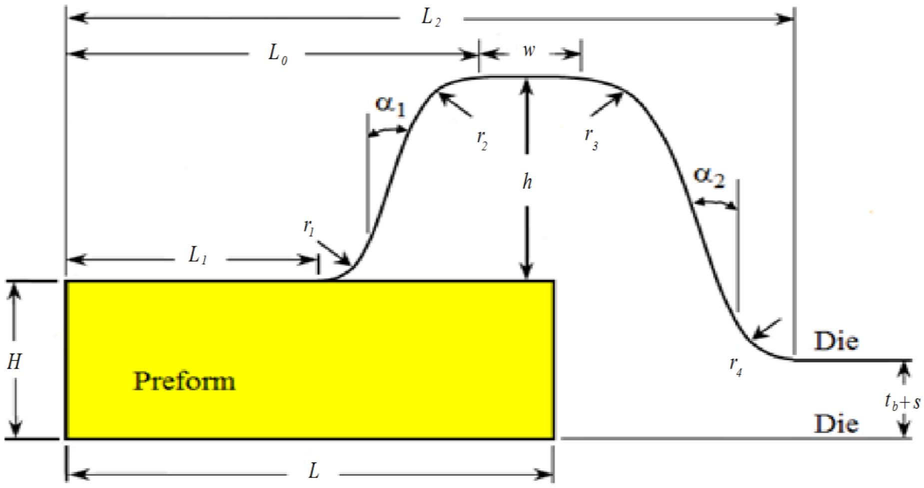

Figure 3.2. Dimensions of quarter part of the I-beam processed by forging [54].

3.2. Formulation of the Objective Function

Solution of an optimization problem first requires definition of an objective function that serve as a criterion for the effectiveness of a design. In this study, the goal is to minimize the overall cost without violating the constraints. Accordingly, the objective function to be minimized is expressed as

$$f = c_m + c_f + c_s + cP \tag{3.1}$$

where c_m is the material cost, c_f is the cost of the forging process, c_s is the cost of the shearing operation, P is the penalty, and c is the penalty coefficient. A suitable value for c was found to be 10. The first three terms have the same unit, which is dollar. The last term takes nonzero value only in case of constraint violations. The costs that are assumed to be independent of the design variables like labor, machinery costs are not included in the objective function.

3.2.1. Material Cost, c_m

The material cost in terms of dollars can be expressed as

$$c_m = p_m \rho V \tag{3.2}$$

where p_m is the unit price of the material in terms of dollars per kilogram, ρ is the density of the material in terms of kg/m^3, V is the volume of material used to produce the part. Considering that the volume of the material does not change with plastic deformation, V can be expressed in terms of the preform dimensions as

$$V = 2H \cdot 2L \cdot L_b \tag{3.3}$$

where L_b is the length of the I-beam. The factor “2” appears because only one fourth of the preform is analyzed (Figure 3.2).

3.2.2. Forging Cost, c_f

The cost of the forging operation is related to the energy spent to deform the workpiece. This energy is assumed to be proportional to the total strain energy of deformation of the final part, U_f, which can be formulated as

$$U_f = \int_0^t \int_V \sigma_{ij} \dot{\varepsilon}_{ij} \, dV \, dt \tag{3.4}$$

where σ_{ij} are the components of the stress tensor and $\dot{\varepsilon}_{ij}$ are the total (elastic and plastic) strain rates. There is sum on i and j. The expression in Eq. 3.5 is not calculated analytically. The strain energy values are kept in the element tables of ANSYS and they are used to calculate U_f.

The cost of forging in terms of dollars as the cost of electricity spent during forging is expressed as

$$c_f = p_e U_f / \eta_f \tag{3.5}$$

where p_e is the local electricity price for industry in terms of dollars/J, η_f is the efficiency with which electricity converted to deformation energy. U_f is four times the strain energy calculated using finite elements, because one fourth of the preform is analyzed.

3.2.3. Shearing Cost, c_s

The post manufacturing cost is related to the energy required to cut the flashes at the sides of the forged part. The shearing energy is calculated analytically using the following formula [55]:

$$U_s = c_{11} c_{22} S_{ut} \left(2t_b\right)^2 L_b \tag{3.6}$$

where c_{11} is a constant equal to 0.85 for ductile materials, c_{22} is a constant equal to 0.5 for soft materials, $2t_b$ is the burr thickness, and S_{ut} is the tensile strength of the material. The cost of the shearing operation is expressed similar to the cost of forging as

$$c_s = 2 p_e U_s / \eta_s \tag{3.7}$$

where η_s is the efficiency of the shearing operation. The factor ‘2’ appears because there is one flash at each side.

3.3. Constraints and Penalty Functions

In typical structural design or processing design problems, a number of constraints need to be imposed on the variables in order to obtain acceptable solutions. This is even more important for design optimization problems to obtain a solution that is optimum as well as feasible. An arbitrary set of values for the optimization variables may not correspond to a feasible geometry. For example, the curvature may not be generated for a negative radius of curvature. The constraints define the feasible domains for the optimization variables. Selection of the constraint limits may be based on the process requirements like the limitations on the manufacturing process, or product requirements like strength and ergonomic considerations. If the feasible domain is arbitrarily restricted, better solutions may be missed. If it is selected unnecessarily large, search for the optimum design may require increased computational effort.

In this study, constraints are imposed on the optimization variables based on the design or process requirements and possible numerical problems in the FE analysis. Behavioral constraints are used to avoid failure of the finished product during service as a design requirement. For the present problem, static failure in the form of yielding and local buckling failure are considered as behavioral constraints. The manufacturing constraints considered in this study are filling of the die cavity, failure of the mold, and limited flash. There are also side constraints like limits on the dimensions of the beam due to spacing requirements, or limits beyond which no feasible design is expected like very small or large fillet radii.

If the constraints are violated, a penalty is added to the objective function. Because the search algorithm tries to find designs with lower objective function values, penalties force the optimization algorithm to search the optimum design only within the feasible domain, where no constraint is violated.

During the optimization process, the value of the objective function is recalculated whenever the values of the optimization variables are changed by the search algorithm. In order to simulate the large deformation during forging, a non-linear FE analysis is performed. One of the problems that may arise is the failure of analysis. The search algorithm may generate a set of variables such that for some reason FE analysis fails, e.g. the geometry may not be constructed due to a negative value assigned to radius of curvature, or analysis may not be completed due to a sharp corner or excessive deformation. If FE analysis fails, objective function cannot be calculated. In such a case, a large penalty value is assigned to the objective function.

In order to avoid underfilling, the distribution of the contact pressure on the punch is obtained after FE analysis; if pressure is zero on some of the elements, a large penalty value is added to the objective function.

The other constraint used in the optimization procedure is the maximum contact pressure on the die, which may cause permanent deformation on the die. If the maximum contact pressure on the punch, $P_{\max}$, exceeds the allowable compressive stress of the mold material, σ_{all}, a penalty is added to the objective function, which is calculated by

$$P = \frac{P_{\max} - \sigma_{all}}{\sigma_{all}} \tag{3.8}$$

If the maximum equivalent stress, $\sigma_{\max}$, developed in the part due to the loads applied during its use exceeds the yield strength of the material, S_y, static failure is predicted; then a penalty is calculated using the following equation:

$$P = \frac{\sigma_{\max} - S_y}{S_y} \tag{3.9}$$

As the formula implies, the higher is $\sigma_{\max}$ above S_y, the higher is the value of the penalty. A similar penalty function is defined for buckling failure.

Consider that for a given optimization variable, x, there is a lower and an upper bound denoted by x_ℓ and x_u respectively. The inequality constraint is expressed as

$$x_\ell < x < x_u \tag{3.10}$$

If the search algorithm assigns a value to this variable outside its feasible range, a penalty is added to the objective function. The nature of the constraint requires that two penalty functions be defined. For the lower bound, the penalty function is defined as

$$P_k = \left\langle \frac{-x + x_\ell}{x_u - x_\ell} \right\rangle \tag{3.11}$$

and the penalty function for the upper bound as

$$P_{k+1} = \left\langle \frac{x - x_u}{x_u - x_\ell} \right\rangle \tag{3.12}$$

Because the type of the penalty functions is external, they become active if their corresponding constraint is violated. Otherwise, they are equal to zero. This condition is controlled by the operator “< >”. If the value of the term inside this operator is positive, it yields the same value, otherwise it yields zero. Note that all of the penalty functions are defined in a manner such that they become zero if their related variable takes a value within its feasible range. Although, burr (or flash) length, L_b, is not variable, upper and lower limits are set to avoid underfilling or excessive material waste, and penalty functions are defined in a similar manner.

3.4. Optimization Procedure

Because of the large number of design variables, a multilevel optimization approach is adopted. In the first level, using the design variables, the part design is optimized. In the second level, using the processing parameters as well as some of the design parameters as optimization variables, the manufacturing process is optimized. After successive runs, product design and process design are finalized.

3.4.1. First Level Optimization

In the first stage of optimization, the material cost is minimized. Because, the preform dimensions are determined in the second level, only the material used in the part, not the material used in the forging process, is minimized. Besides, manufacturing cost, which is calculated in the second level, is not included. In objective function of the first level the height of the web, h_w, the width, *b*, the thicknesses of the web, t_w, and the flange, t_f, are used as design variables. To calculate material cost price of material, density and volume of I-beam is used in the function.

$$f = p_m \rho V_p + P \tag{3.13}$$

where P is the penalty, p_m is the unit price of the material, ρ is the density, V_p is the volume of the part. If V_p is expressed in terms of the geometric parameters shown in Figure 3.1 and substituted, the equation becomes

$$f = p_m \rho \left(2bt_f + h_w t_w\right) + P \tag{3.14}$$

The design parameters, t_f, t_w, h_f, *b*, affecting the objective function are chosen as optimization variables in the first level. The behavioral constraints, static failure and buckling failure, as well as side constraints are used. The side constraints are the chosen upper and lower limits on the optimization variables. The limits are given in Table 3.2. The upper limits on h_f and *b* are chosen based on spacing requirements. The other limits are chosen such that beyond them no feasible solution is expected; they just serve to limit the search domain in order to avoid unnecessary calculations. Initially, fillet radii are taken as 3 mm; in the next iterations, the optimum values found in the second level are used.

Table 3.2. The upper and lower limits (in mm) on the variables in the first level.

$20 \le h_f \le 45$
$10 \le b \le 35$
$0.5 \le t_f \le 20$
$0.5 \le t_w \le 20$

3.4.2. Second Level Optimization

In second level, the total cost of the I-beam including the material, forging, and shearing costs is optimized. Accordingly, the expression in Eq. 3.14 is used as the objective function. The thickness of the flange, t_f, the thickness of the web, t_w, and the width, *b,* are considered as constants. Their values optimized in the first level are adopted in the second level. On the other hand, height of the web, h_w, fillet radii, r_1, r_2, r_3, and r_4, half of the preform dimensions, *H* and *L*, and half burr thickness, t_b are considered as optimization variables in the second level. The only variable considered as optimization variable in both levels is the height of the web, h_w, All of the aforementioned constraints are imposed in the second level including behavioral constraints, i.e. static failure and buckling failure.

Table 3.3 shows the upper and lower limits on the constrained parameters. All of these parameters are optimization variables except ℓ in Eq. 3.15. The range of allowable values limits are selected as wide as possible. Beyond the limits, difficulties in generating the shapes and FE solutions are observed.

Table 3.3. The upper and lower limits (in mm) on the parameters in the second level.

$1 \le r_1 \le 7$
$1 \le r_2 \le 7$
$1 \le r_3 \le 7$
$1 \le r_4 \le 7$
$11 \le L_o \le 19$
$0.5 \le t_b \le 8$
$14 \le H \le 24$
$0 \le F_l \le 2$
$-0.9 \le \ell \le 1.1$

3.5. Search Algorithm

Various search algorithms were preferred in previous studies of forging process optimization. Chung and Hwang [15] applied to genetic algorithm, Byon and Hwang [60] applied to derivative-based approach and Doltsiniz *et al.* [64] and Zhao *et al.* [25] applied to sensivity analysis and Bonte *et al.* [43] applied to Sequential Approximate Optimization to formulate the process optimal design.

One of the earliest methods, gradient based approach, used in forging optimization problems using Finite Element simulations. Conjugate Gradient is one of the classical iterative optimization algorithms in which difficulties to obtain sensitivities and avoiding local optima is encountered [43]. Derivatives of the objective function with respect to design variables are required in this method. Different methods used for the calculation of the derivatives which called sensitivity analysis. The sensitivity analysis can be difficult due to differentiation of complex equations or the discontinuity of the objective function. When a large number of design variables used in the optimization function more effort needed to be performed and complex calculations needed to be done [3].

The other common optimization algorithm is evolutionary method including genetic algorithm which depends on direct search approach. This method is developed with the utilizing biological logic; inheritance, mutation, selection, and crossover in each iteration. Genetic algorithms do not require any derivatives. However FE simulations are applied due to the need for large number of metal forming simulations for representative solutions thus there will be high computaitonal cost [3]. Although this method seems beneficial for optimization problems, large number of finite element simulations and many function evaluations are needed to be done [15, 43].

Due to the difficulties of derivations and sensitivity data in gradient methods and the requirements for time consuming finite element simulations in genetic algorithms, different approximation methods such as response surface method (RSM) have been used for more feasible solutions [3]. In these methods there is tendency to find global optima and no need for sensitivities and differentiation of equations. Approximation methods result in computational efficiency with less number of simulations compared to genetic algorithm and without using derivatives which is the basic issue for gradient based methods. However results depend on the model and objective function [43]. Thus this method is only feasible for sheet metal forming and clinching forming optimization problems [3].

On the other hand direct search methods examine and compare less trial and sampling solutions before determination of the best possible search directions in the next iteration. Direct search methods are more preferable for metal forming processes due to the lack of derivations and requirement for small number of sampling [3].

In this study, Nelder-Mead algorithm, one of the direct search algorithms, is selected as the search algorithm because it is a robust zero-order search algorithm not requiring numerical derivatives of the objective function. As mentioned before, FE analysis fails for some configurations generated by the search algorithms. In these cases, objective function can not be calculated; for this reason a large penalty value is assigned to the objective function. Even though higher order search algorithms are more efficient, noting that derivatives can not be calculated for some configurations, they are not suitable for use in the solution of the present problem.

At the beginning of the optimization procedure objective function is analytically expressed and then variables and constraints are defined before choosing the appropriate search algorithm for the optimization. Weighting constants are applied to synchronize the units in objective function. In this thesis Nelder-Mead Algorithm in which derivation of equation is not required is choosen as optimization algorithm.

In this algorithm n+1 set of objective function values are selected and calculated for a function having n variables. Assuming, a simplex is a triangle, having two variables and the method is a pattern search that compares function values at the three vertices of the triangle. Worst or biggest vertex rejected and replaced with a new vertex which has a better objective function value. By obtaining a new triangle search is continued. The process finds new triangles (which have different shapes), for which the function values at the vertices get smaller and smaller. The aim is to reduce the size of the triangle and to obtain the variable values of the minimum point.

Mainly random points in feasible domain are selected by the optimization code at the beginning. These points are controlled after creating initial geometries to prevent finite element errors and failures. If errors and failure occur for these values, new ones are randomly selected until error-free values are obtained. Then initial geometry is created and loads, boundary conditions and material properties are applied on finite element model. Resuts of finite element analysis, mainly energy and geometric calculations are used in objective function calculations. To have relevant terms in objective function weight constant is multiplied to terms to have objective function terms which have same magnitude. After terms are prepared in function, penalty terms are added. Generally penalties are activated when variable violates the limits of feasible range, failure occurs under working conditions and finite element analysis fails. If desired limits are violated in analysis, penalty function is applied according to extention of limits. Figure 3.3 shows the flow chart of optimization process.

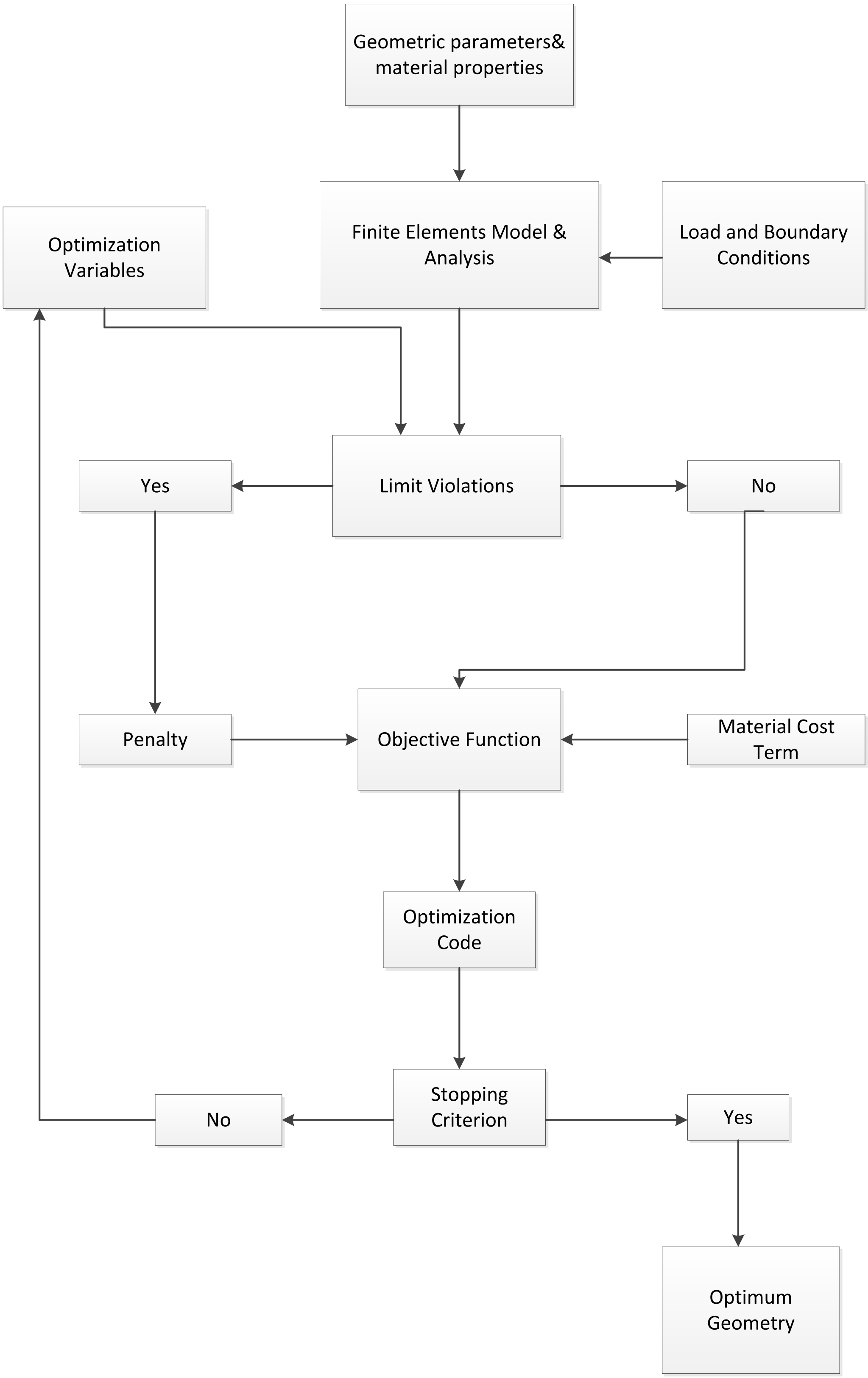

Figure 3.3. Flow chart of the optimization process.

A built-in ANSYS code is developed to integrate the finite element model and the algorithm. This program carries out the finite element analysis and writes the results into output files. Program finds new values and calculates the objective function until the predetermined convergence criterion is satisfied and optimum values are obtained.

3.6. Finite Element Modeling

3.6.1. First Level Model

In the first level optimization 3D model is used due to design in which radii in flange and web takes place. During the study FE model is integrated to the optimization code in which values are evaluated by the Nelder-Mead algorithm.

3.6.1.1. Meshing and Elements. Selecting an appropriate element and meshing the model is the most important part of obtaining reliable results. Due to having radii in I-beam and using 3D model in the shape optimization tetrahedral option of SOLID 95 is selected as element type as shown in Figure 3.4. It can tolerate irregular shapes without as much loss of accuracy. SOLID95 elements have compatible displacement shapes and they are well suited to model curved boundaries.

The element is defined by 20 nodes having three degrees of freedom per node: translations in the nodal x, y, and z directions. The element may have any spatial orientation. Moreover SOLID95 has plasticity, creep, stress stiffening, large deflection, and large strain capabilities.

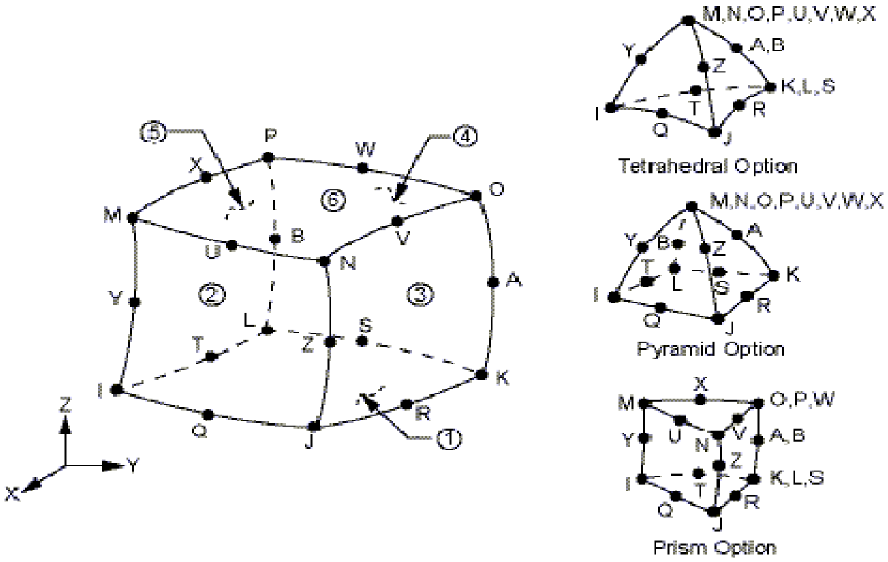

Figure 3.4. SOLID95 with its 20 nodes [65].

According to the need to calculate stress in the part, I-beam is meshed as a volume. The amount of mesh elements are evaluated during the analysis according to the required time and the convergence of results.

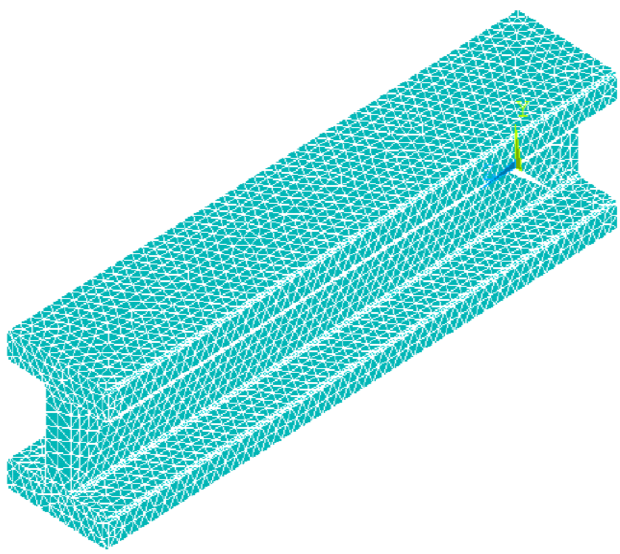

Figure 3.5. Meshed I-beam [65].

<u>3.6.1.2. Material Model.</u> In ANSYS users have ability to choose the material model due the needs of their studies. Designers can choose constant, isotropic, linear material properties from a material library available through the GUI. Young's modulus, density, coefficient of thermal expansion, Poisson's ratio, thermal conductivity and specific heats are available for 10 materials in four unit systems [65]. In this study the selected material model is linear elastic isotropic model.

<u>3.6.1.3. Boundary Conditions.</u> In the FE model, there are both displacement and force applied on nodes as can be seen in the Figure 3.5. In the cost optimization of material ends of I-beam are restrained from moving along the y axis and mid-ends are restrained from moving x any y axis. Force is applied on the top area at the mid nodes of I-beam as can be seen from Figure 3.6.

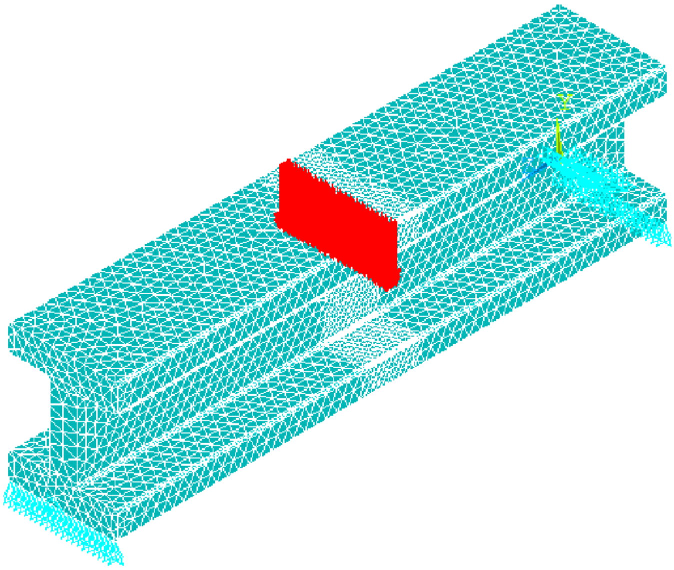

Figure 3.6. Boundary conditions applied on the I-beam [65].

3.6.2. Second Level Model

Selection of an appropriate element type, meshing, contact elements, boundary conditions, and material model in the analysis are significant for obtaining true results. In the cost optimization of the total cost, maximum von mises stress and maximum von mises strains are chosen to control result parameters. First and second level optimization differs in modeling of the part in the finite element analysis. For the total cost optimization level 2D model is designed instead of 3D model which takes more computational effort and time.

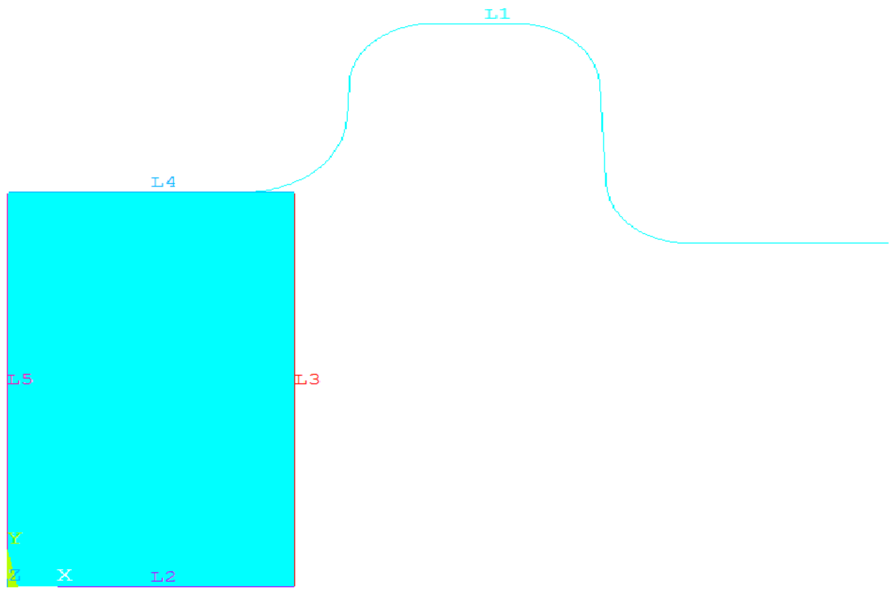

Figure 3.7. FE Model in Ansys.

3.6.2.1. Meshing and Elements. The element type chosen for workpiece is Plane183, being a high order, 8-node 2D rectangular element as can be seen in Figure 3.8. Moreover the element should have large deflection, large strain capabilities. Therefore a high order element is more suitable for highly nonlinear deformation. In this thesis one of the I-beam dimension is significantly longer than other dimensions and I-beam is subjected to only lateral load. According to these dimensions and load application plain strain idealization is valid for I-beam case. Therefore in the second level optimization the element type chosen for workpiece is Plane183 using plain strain option.

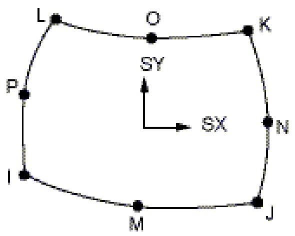

Figure 3.8. PLANE183 with its 8 nodes [65].

In order to determine the mesh density a convergence analysis will be carried out select appropriate element size.

<u>3.6.2.2. Contact Elements.</u> Rigid-to-flexible and surface-to-surface contacts are used in this level of study. The workpiece is a deformable contact body and the dies and punch are defined as rigid target bodies. The boundary lines of the bodies have to be meshed in order to establish contact pairs. For this purpose, CONTA172 was selected for the deformable lines, and TARGE169 was selected for the non-deformable lines. In order to create a contact, the groups of nodes which probably come in contact were specified.

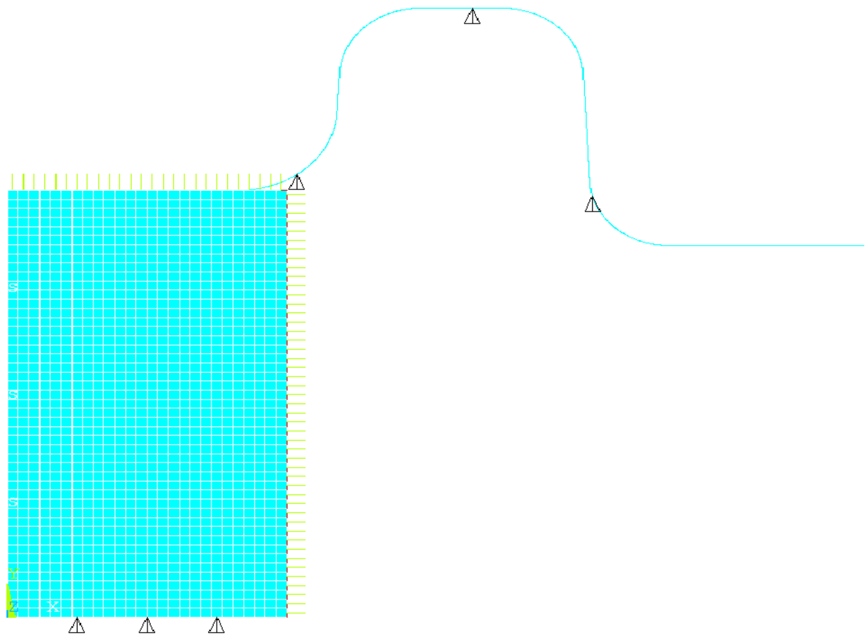

Figure 3.9. Meshed FE model with contact pairs and boundary conditions.

Figure 3.9 shows the last shape of model before stroke is applied. Contact is determined between lines L1 and L4 which is depicted in Figure 3.7. This contact is rigid to deformable.

<u>3.6.2.3. Boundary Conditions.</u> In the FE model, according to the boundary conditions there are only displacement boundary conditions and symmetry boundary condition applied on lines. Friction forces exist between the contacting surfaces impeding movement.

The punch lines are restrained from rotating and moving along the *x*-axis but allowed to move through the vertical displacement which is defined with the equation below.

$$s = H - h_s \tag{3.15}$$

where *H* is height of preform and applied as a design variable limited between 14 and 24.

3.6.2.4. Friction Coefficient. After creating geometry, friction coefficient is selected before finite element simulations are applied. Zhao *et al.* [25] took 0.2 as friction factor. However smaller values assist die full-fillment and prevent cavities. Therefore different coefficients are applied for same geometries to compare occurance of cavities. Figure 3.10 shows the finite element results for the same geometric parameters and in these analysis friction coefficients are 0.5, 0.05, and 0.005 respectively. According to these finite element results variations and die cavities in results are not observed. Therefore iterations started with using 0.05 as friction coefficient and for the optimum design 0.2 is applied to check the full-fillment according to friction coefficient.

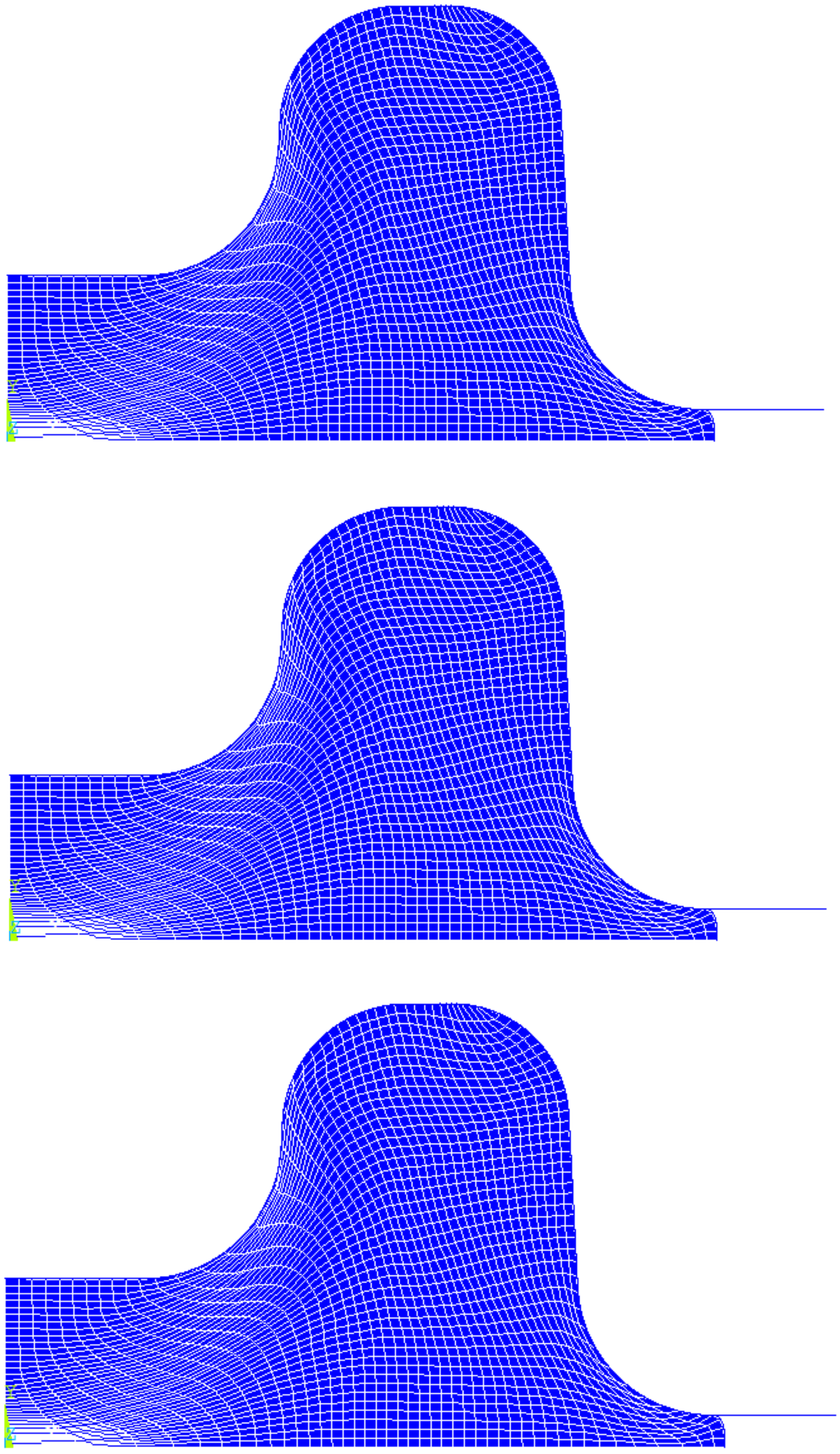

Figure 3.10. Finite element results of I-beam for same geometric parameters with different friction coefficients.

3.6.2.5. Material Model. Various material models are available for 2-D, beam, shell, brick and tetrahedral elements. Nonlinear material models are used when an elastic material is going to be loaded past the yield strength of the material. When this happens, plastic deformation will occur. There are two types of hardening material models available. The isotropic hardening model involves yielding the entire yield surface uniformly. However kinematic hardening in which Bauschinger effect is included involves a shifting of the yield surface (primarily due to a reversal of loading) and this model is preferred for analyses involving cyclical loading.

Multilinear curve is used instead of a bilinear curve in Multilinear Isotropic Hardening Material Model (MISO). This model is not recommended for cyclic or highly nonproportional load histories in small-strain analyses. It is, however, recommended for large strain analyses. The MISO option can contain up to 20 different temperature curves, with up to 100 different stress-strain points allowed per curve. Strain points can differ from curve to curve. Also combining MISO with nonlinear kinematic hardening model allows simulating cyclic hardening or softening. However for the I-beam case there is no need for this combination. The part considered in this study is manufactured through forging in which loading and unloading the preform is applied. However these conditions should not be considered as cyclical loading because of performing them once.

In this study, the selected material model is multi-linear isotropic hardening (MISO) model. MISO is a rate independent model suitable for large strain applications. In MISO, the stress–strain curve is described by a set of linear sub-elements instead of a power equation. Using the datum points from the experimental stress-strain curve, the stress-strain curve used in the nonlinear analysis is defined. To obtain better non-linear curve, more points are needed. The MISO flow curve of SAE 1010 created by ANSYS using the 30 datum points [66] from the materials flow curve as can be seen in the Figure 3.11.

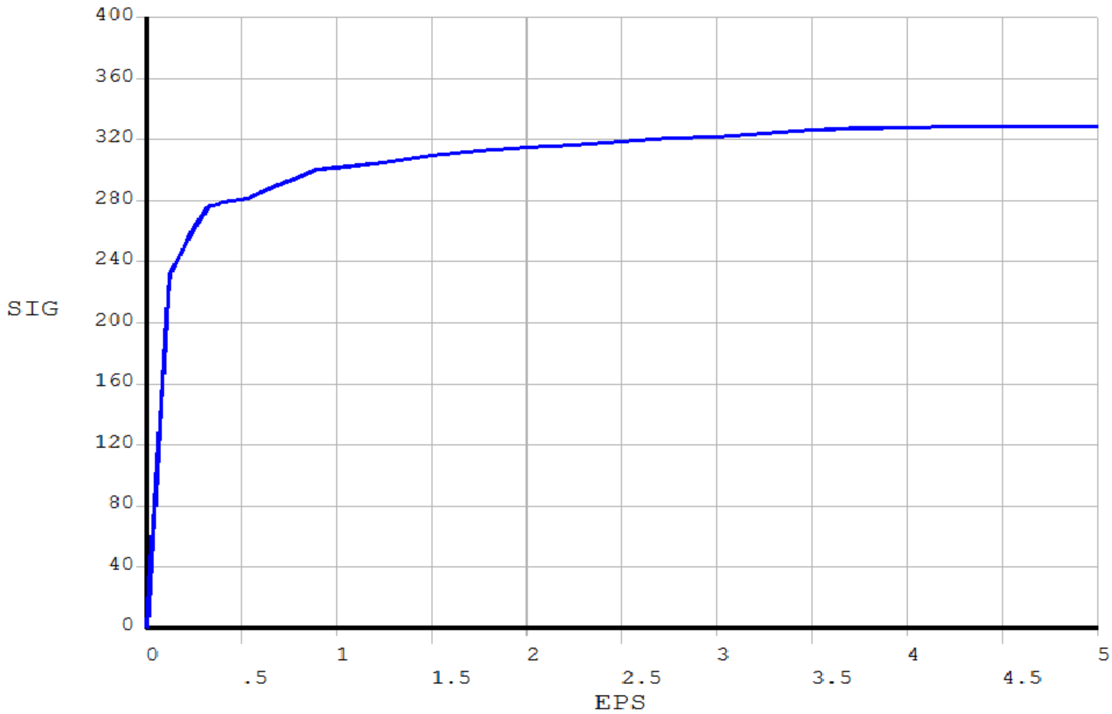

Figure 3.11. MISO flow curve of SAE 1010 generated in ANSYS [65].

3.7. Structural Analysis

3.7.1. Yield Strength after Forging

Because of work hardening of the material during the forging process, yield strength of the undeformed material used in forging, SAE 1010, changes. For this reason, the yield strength of the deformed material should be used in the failure analysis and design of of the part. In this study, the modified yield strength is calculated at the critical locations, where failure is possible, by obtaining the true stress distribution at the end of the forging process using finite element analysis and converting them to engineering stress at those locations.

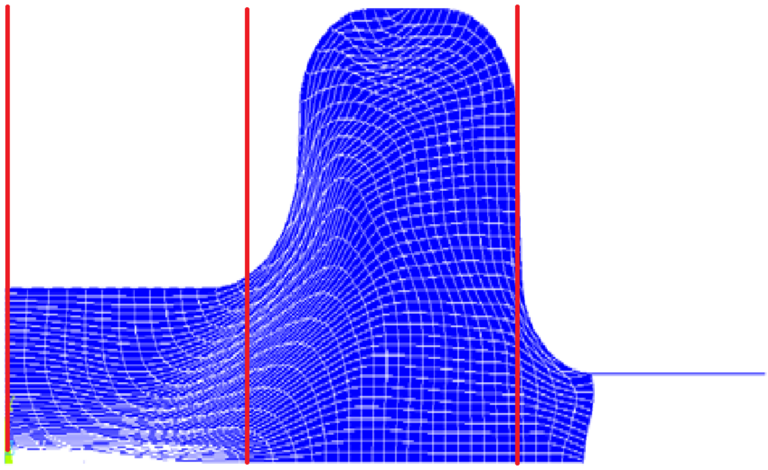

Figure 3.12. Expected failure locations in the I-beam.

Red lines in Figure 3.12 show the locations where failure is possible for an I-beam under transverse load. Top of the I-beam is a critical failure location because the maximum stress, Mc/I, develops in this region. The interface between the flange and the web is also inspected, because bending stress is combined with shear. The center of the I-beam is checked for possible failure due to the maximum shear stress.

By simulating the forging process by FEM, equivalent stresses along these lines are obtained; then the averages of these values are calculated. Using the equation below the true stress values are converted to engineering stress.

$$\sigma_E = \frac{\sigma_T}{e^{\varepsilon_T}} \tag{3.16}$$

where σ_T is the true stress, ε_T is the true strain, σ_E is the engineering stress, which is used as the yield strength of the material at the corresponding line if it is larger than the yield strength of the undeformed material. If the maximum stress that develops at a given point during forging does not exceed the yield strength of the material, S_y, one may assume that the yield strength of the material at that point does not change. Accordingly, the yield strength can be taken as 305 MPa for SAE 1010 after forging. Otherwise, it should be taken as σ_E .

$$S_y = \sigma_E \quad if \quad \sigma_E > S_y \tag{3.17}$$

However, residual stresses developed in the part during forging should also be taken into account in the structural analysis.

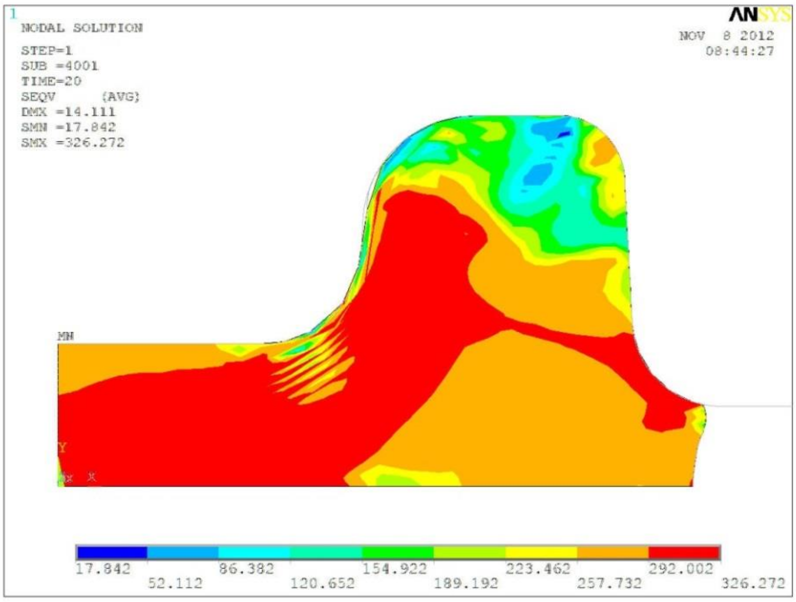

Figure 3.13. Von Mises Stress distribution after loading.

The average true Von Mises stress at the top and bottom is obtained to be about 230 MPa. On the other hand, the stress between the flange and the web is 290 MPa, and the stress on the flange is 290 MPa as can be seen from Figure 3.13. The corresponding engineering stress values are 188 MPa, 130 MPa, and 109 MPa respectively.

3.7.2. Residual Stress Calculations

Residual stresses developed during the forging process may affect the failure response of the beam during its use. Therefore, they should be accounted in the analysis and design of the beam.

In order to correctly evaluate the residual stresses after the removal of the upper die, kinematic strain hardening rule is used instead of isotropic hardening in the finite element model of the forging process. The same procedure described above is applied; but after the first loading, i.e. downward displacement of the punch by *s*, the punch is moved upward. After the removal of the load, the resulting stress state represents the residual stress state. Figure 3.14 shows the stress distribution in z direction after unloading.

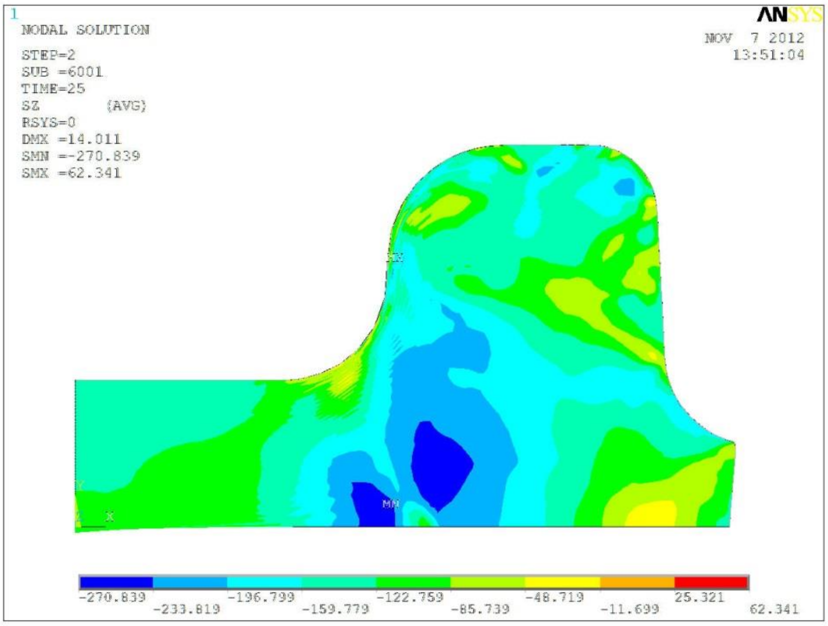

Figure 3.14. Residual stresses in the z direction after unloading.

The residual stresses at the top and bottom are obtained to be about 120 MPa. On the other hand, the residual stress between the flange and the web is 160 MPa, and the residual stress on the flange is 120 MPa as can be seen from Figure 3.14. They are all compressive. Using Equation 3.17 engineering residual stress values at these points are calculated as 105, 137 and 105 respectively. After converting to engineering stress, the residual stress, σ_r, is subtracted from the yield stress, S_y, to calculate the new yield stress according to following equation:

$$S_y^{\mathrm{I}} = S_y - \sigma_r \tag{3.1}$$

Subtracting the residual stress values from yield stress, engineering stresses are calculated as 200 MPa at the top and bottom points of I-beam, 200 MPa on web, 168 MPa between the flange and web.

3.7.3. Failure Analysis of the I-Beam during Its Use

If the equivalent stress, σ_{eq}, developed in one region of the part during its use exceeds the yield stress, S_y^{I}, at that region, static failure is predicted; then a penalty is added to the objective function.

A structural analysis is required to predict whether static and buckling failures will occur in the part during its use. For this purpose, an analysis based on Bernoulli-Euler beam theory is carried out. The maximum normal stress, $\sigma_{\max}$, develops at the top and bottom of the beam at the section where the bending moment takes its maximum value, $M_{\max}$. $\sigma_{\max}$ can be calculated using the following well known formula:

$$\sigma_{\max} = \frac{M_{\max} c}{I_{zz}} \tag{3.2}$$

where c is the distance between the neutral axis and the furthermost point. The geometry of the cross section of the I-beam is shown in Figure 3.15. Accordingly, c is equal to $h_f / 2$.

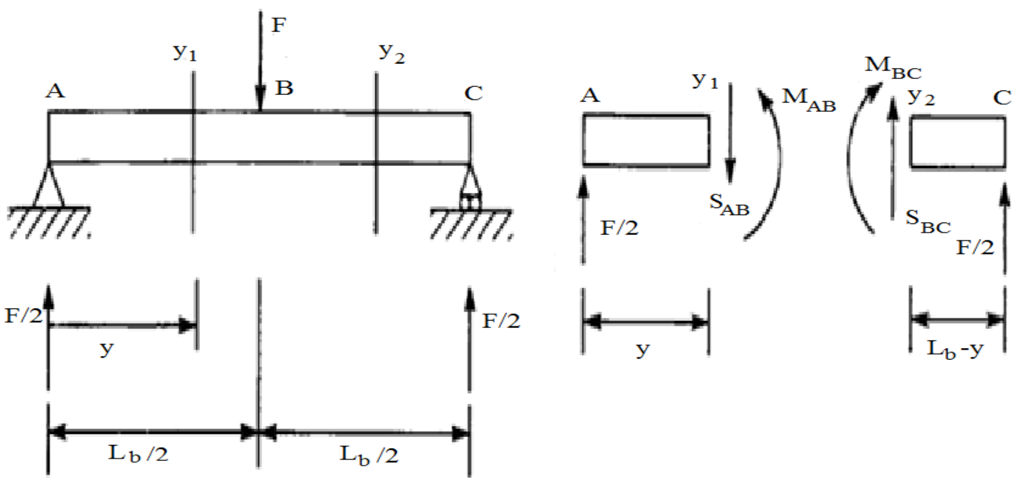

Figure 3.15. Loading condition [56].

The maximum bending moment, $M_{\max}$, develops at the middle of the beam with a magnitude of

$$M_{\max} = \frac{FL_b}{4} \tag{3.3}$$

where F is the force applied at the middle of the beam as the worst loading condition during its use. F already includes the safety factor for uncertainties regarding its magnitude. The area moment of inertia of the I-beam with respect to the z-axis, I_{zz}, is given as

$$I_{zz} = \frac{bh_f^{\,3}}{12} - \frac{(b - t_w)h_w^{\,3}}{12} \tag{3.4}$$

here the fillets or draft angles are not considered. If the radii of the curvatures are taken into account, the formula becomes.

$$\begin{aligned}
\mathrm{I}_{zz} &= 2\left\{\frac{1}{12}(b - 2r_3)t_f^{\,3} + \left[t_f\,(b - 2r_3)\right]\left(\frac{h_w + t_f}{2}\right)^2\right\} \\
&+4\left\{\frac{\pi}{16}r_3^{\,4} + \frac{\pi r_3^{\,2}}{4}\left(\frac{h_f}{2} - r_3 + \frac{4r_3}{3\pi}\right)^2\right\} + 4\left\{\frac{\pi}{16}r_2^{\,4} + \frac{\pi r_2^{\,2}}{4}\left(\frac{h_w}{2} + r_2 - \frac{4r_2}{3\pi}\right)^2\right\} \\
&+4\left\{\frac{1}{12}r_3\left(t_f - r_3 - r_2\right)^3 + r_3\left(t_f - r_3 - r_2\right)\left(\frac{h_w + t_f}{2}\right)^2\right\} + \frac{1}{12}t_w h_w^{\,3} \\
&+4\left\{\frac{r_1^{\,4}}{12} + r_1^{\,2}\left(\frac{h_w}{2} - \frac{r_1}{2}\right)^2 - \left[\frac{\pi}{16}r_1^{\,4} + \frac{\pi r_1^{\,2}}{4}\left(\frac{h_w}{2} - r_1 + \frac{4r_1}{3\pi}\right)^2\right]\right\}
\end{aligned} \tag{3.5}$$

The shear stress at the intersection between the web and flange is calculated by

$$\tau = \frac{VQ}{I_{zz}t} \tag{3.6}$$

where Q is given by

$$Q = bt_f \frac{h_w + t_f}{4} \tag{3.7}$$

where τ is the shear stress, V is the shear force, t is the thickness and Q is the first moment with respect to neutral axis of the portion of cross section.

Equivalent stress is obtained as following:

$$\sigma_{eq} = \sqrt{\left(\frac{\frac{WL_b}{4}\frac{h_w}{2}}{I_{zz}}\right)^2 + 3.\left(\frac{Vbt_f\frac{h_w + t_f}{4}}{I_{zz}t}\right)^2} \tag{3.8}$$

The shear stress in the middle region of the beam is approximately calculated as:

$$\tau = \frac{V}{h_f t_w} \tag{3.9}$$

The allowable shear stress is calculated based on the equivalent stress.

$$\tau_{allow} = 0{,}577S_y \tag{3.10}$$

where V is the shear force, h_f is the height of the beam, t_w is the thickness of the web, τ_{allow} is the allowable shear stress and S_y is the yielding strength.

3.7.4. Lateral Buckling

Lateral buckling may occur in beams subjected to transverse loads or bending moments when the critical load is exceeded. The lateral buckling is accompanied by twisting of the beam with respect to the principal axes of inertia. With assumption of lateral buckling, critical load is calculated [57].

$$F_{cr} = \frac{4\pi^2}{l^2}\sqrt{\frac{3}{\pi^2+6}EI_w\left(GJ+\frac{EC_1\pi^2}{l^2}\right)} \tag{3.11}$$

where E is the modulus of elasticity, which is equal to 205 GPa [58], G is the shear modulus of elasticity, which is equal to 80 GPa [58], I_w [55] is torsion warping constant, and J is torsion constant.

$$I_w = \frac{I_{yy}h_w^{\ 2}}{4} \tag{3.12}$$

$$J = \frac{1}{3}\sum m_i t_i^{\ 3} \tag{3.13}$$

For I-beams torsion constant is obtained as follows:

$$J = \frac{2bt_f^{\ 3} + \left(h_w + t_f\right)t_w^{\ 3}}{3} \tag{3.14}$$

Moment of inertia is used in the equation above and calculated as following

$$\begin{aligned}
\mathrm{I}_{YY} &= 2\frac{1}{12}\left(b-2r_3\right)^3 t_f + 4\left\{\frac{1}{3}\left[t_f - r_3 - r_2\right]r_3^{\ 3} + \left[t_f - r_3 - r_2\right]r_3\left(\frac{b-2r_3}{2}\right)^2\right\} + \frac{1}{12}h_w t_w^{\ 3} \\
&+4\left\{\frac{\pi}{16}r_3^{\ 4} + \frac{\pi r_3^{\ 2}}{4}\left(\frac{b}{2} - r_3\right)^2\right\} + 4\left\{\frac{\pi}{16}r_2^{\ 4} + \frac{\pi r_2^{\ 2}}{4}\left(\frac{b}{2} - r_2\right)^2\right\} \\
&+4\left\{\frac{1}{3}r_1^{\ 4} + r_1^{\ 2}\left(\frac{t_w}{2} + r_1\right)^2 - \left[\frac{\pi}{16}r_1^{\ 4} + \frac{\pi r_1^{\ 2}}{4}\left(\frac{t_w}{2} + r_1\right)^2\right]\right\}
\end{aligned} \tag{3.15}$$

Steel punches are limited to approximately 1200 MPa and cobalt-bonded WC punches are limited to approximately 3300 MPa. In this study maximum contact pressure on die is permitted up to 1200 MPa [59].

Moreover optimization results show less flash volume results in less burr and energy need for shearing. Altough material loss is prevented with small flash volume, a cavity usually develops in the part as seen in Figure 3.16 when the flash volume is less than 0.

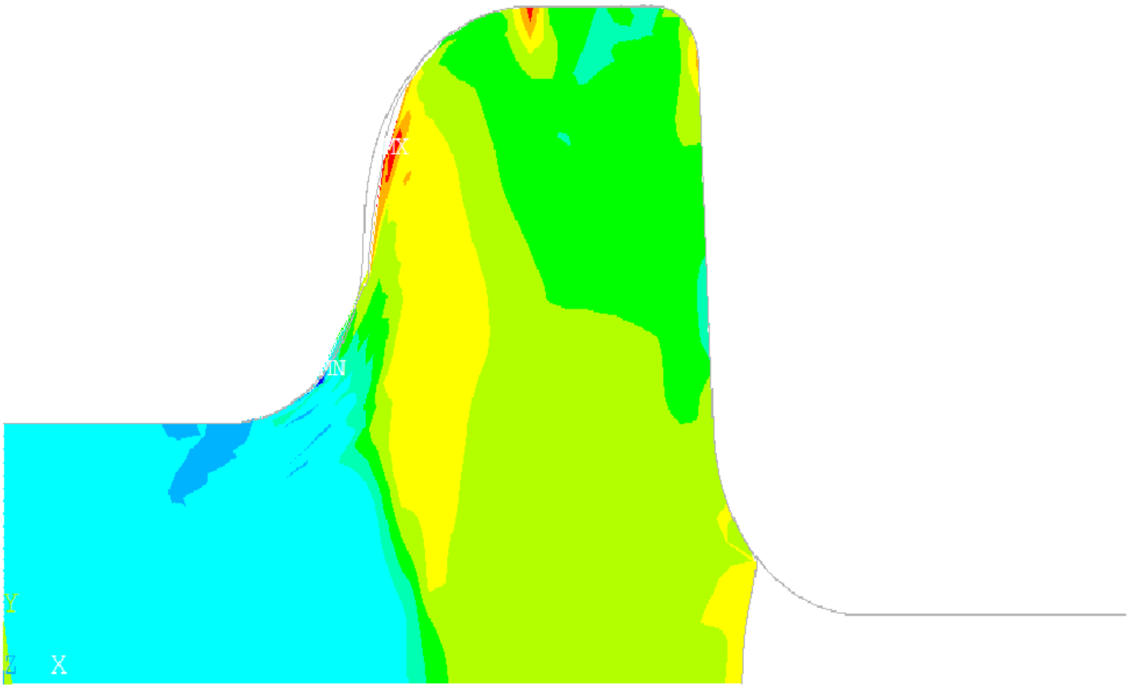

Figure 3.16. Von misses stress distribution of the part including cavity.

Therefore preventing cavities and thus having defectless part is a significant criterion in the design. To prevent the cavities, the code examines the pressure on die. Using the cavity examining part of the ANSYS built in code, the parts which include cavities are eliminated before the Nelder-Mead algorithm starts.

3.8. Convergence Analysis

Results are reliable when there is a possibility to compare them with other experimental results or theoritical data. In this study because of finite element model hand calculations are not really possible and desired. On the other hand convergence analysis and comparison between results of different element sizes or substeps lead to choice of settings to obtain reliable results. Applying convergence analysis designer can compare results according to different settings and impacts of these settings on results.

3.8.1. Convergence Analysis of First Level

In ANSYS warning messages guide the users to find the appropriate settings. However in some cases solution settings such as iteration number, element size or substep number affect the results. In this study Maximum von Mises stress is chosen to be the control result parameters and the proper settings are obtained after convergence analysis. The analyses are repeated for mesh sizes from 6 to 2 for F=42000 N, $t_f = 12$ mm, $t_w = 12$ mm, $b = 40$ mm, $h_f = 40$ mm. Corresponding results are given in Table 3.4.

Table 3.4. Maximum von Misses stresses corresponding to different element sizes.

Element Size	Maximum Stress
6	308.28 MPa
5	307.54 MPa
4	308.48 MPa
3	308.11 MPa
2	308.11 MPa

As it can be seen from the Table 3.4 the element size of 3, for which the values are settling, seems to be an acceptable value for FEM.

Table 3.5. Maximum von Misses stresses corresponding to different refinement sizes.

Refinement	Maximum Stress
2	308.11 MPa
1	308.11 MPa

Refinement can be made to obtain more proximate results. At the mid length of I-beam volume for element size 3 an analysis for refinement size 2 and 1 are made. However

Table 3.5 shows that using element size 3 without any refinement is acceptable for this study.

Moreover applying to finite element simulations in each stage of optimization makes the analysis time consuming. Therefore results of convergence analysis compared with the hand calculations for the stress values. Similiar stress values are obtained from hand calculations and finite element results. Due to obtaining same values finite element method is not applied in each iteration step. Instead of finite elements hand calculations are applied to provide an analysis with less time.

3.8.2. Convergence Analysis of Second Level

In ANSYS warning messages guide the users to find the appropriate settings. However in some cases solution settings such as iteration number, element size or substep number affect the results. In this study Maximum von Mises stress and Maximum von Mises strainare chosen to be the control result parameters and the proper settings are obtained after convergence analysis. The analysis are repeated for mesh sizes from 0.8 to 0.2 for the parameter values r_1 =3.348, r_4 =2.818, t_b =0.576, L_o =14.031, H =17.713 used in the analysis. Corresponding results are given in Table 3.6.

Table 3.6. Maximum Von Misses stresses and strains corresponding to different element sizes.

Element Size	Maximum Von Misses Stress	Maximum Von Misses Strain	Result
0.8	740.40	0.13860	3.61610351
0.7	756.51	0.15228	3.61611874
0.6	777.39	0.11554	3.61611415
0.5	777.87	0.13102	3.61609764
0.4	771.33	0.13632	3.61607752
0.3	770.21	0.14581	3.61605493
0.2	769.86	0.15473	3.61604207

As it can be seen from the Table 3.6 the element size of 0.4, for which the values are settling, seems to be an acceptable value for FEM. However in this level iterations started with the element size 0.4 and after 10 iterations element size 0.2 is applied to obtain more accurate results. Figure 3.17 and Figure 3.18 show the forging process simulations using the trial value of 0.4 for element size.

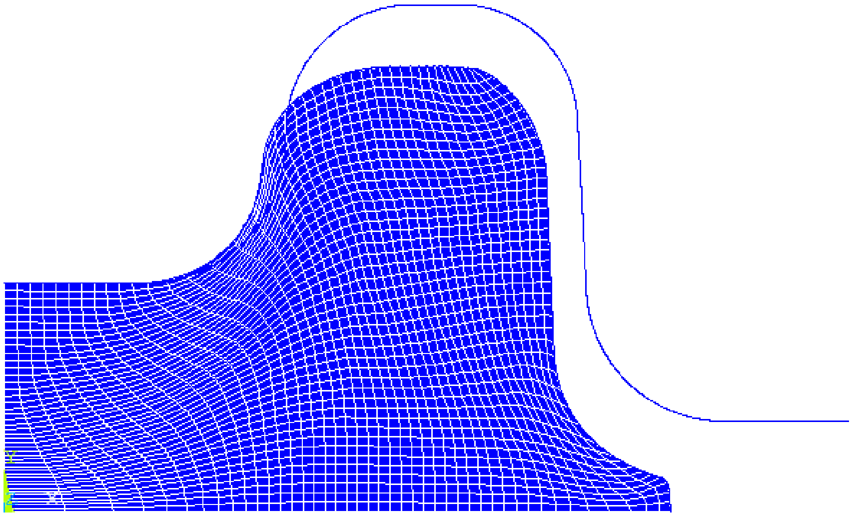

Figure 3.17. Part at the middle stage of the process.

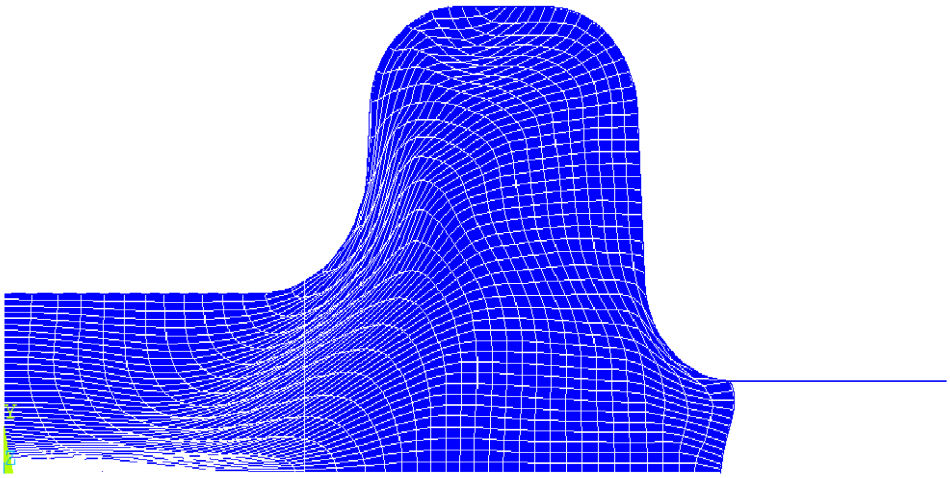

Figure 3.18. Last view of animation.

Different substep numbers are applied to obtain error-free and less time consuming results. Starting from 500, different values are given for minimum and maximum substep numbers. According to the deformation warnings 6000 is selected for initial, 8000 for maximum and 4000 is selected for minimum number of substeps for the analysis.

In this study there are two stages including concurrent design and process optimization in forging. In the first level of optimization shape optimization of the I-beam is aimed. In the second level of optimization cost optimization including material cost, forging cost and shearing cost is aimed.

4. RESULTS AND DISCUSSIONS

Optimization process is divided into two stages to foresee the effects of dimensional parameters in first place and then optimization is extended in which manufacturing and postprocess parameters included. First level optimization includes cost of cross-sectional area of the I-beam minimization and second level includes minimization of total cost of the forging process containing material cost, forging cost and shearing cost. After determining effect of dimensional parameters on material cost in first stage, total cost is minimized in second stage.

Optimization is performed in two phases; material cost optimization and total cost optimization. Manufacturing and behavioral constraints are used to ensure safe use of I-beam. Failure conditions due to static yielding and local buckling, die filling, maximum allowable pressure on die, limited flash out of die are limited to fill up the billet, prevent failure of dies and material waste. Dimensions of the I-beam, fillet radii, thickness of the flash and preform dimensions are the variables in the optimization.

Steel 1010 is the material of the forging process and total cost is calculated including material and manufacturing cost.

4.1. First Level Optimization Results

Optimization in the first level is done for four variables; the height, and width of the beam and thicknesses of flange and web while the radii. The upper and lower limits are defined for the variables and used in the penalty function. The lower and upper limits defined for h_f are 20 and 45, the lower and upper limits defined for b are 10 and 35, the lower and upper limits defined for t_f are 0.5 and 20, the lower and upper limits defined for t_w are 0.5 and 20. In the first iterations the values for radii r_1 =1, r_2 =1, r_3 =1 and r_4 =1 are applied.

Table 4.1. Results of the first level optimization.

	h_f	b	t_f	t_w	Cost
1	44.97	34.89	18.81	19.94	1.813
2	45.00	34.99	10.43	16.19	1.392
3	45.00	34.92	10.24	17.47	1.421
4	45.00	32.36	17.48	7.98	1.506
5	33.03	26.07	2.74	9.29	279.881
6	45.00	34.43	11.70	13.31	1.358
7	44.99	34.99	11.01	13.27	1.336
8	44.81	34.90	12.14	12.21	1.364

Iteration results are shown in the Table 4.1. Optimum cost is 1.336 which is obtained in the seventh iteration. Values for parameters in second level are taken according to the seventh iteration results which are 44.99 for h_f, 34.99 for b, 11.01 for t_f and 13.27 for t_w.

4.2. Second Level Optimization Results

Different cases are compared in the second level optimization case. Firstly, optimizations are conducted for fewer variables; radii and burr thickness and half height of web. Then preform dimensions are also included as optimization variables due to the need of finding optimum preform. Besides burr thickness and burr volume are taken as optimization variables to avoid flash and to minimize overall cost.

The range of permissible values for r_1 is from 1 to 7, for r_2 is from 1 to 7, for r_3 is from 1 to 7, for r_4 is from 1 to 7, for L_o is from 11 to 19, for t_b is from 0.5 to 8, for H is from 14 to 24,and for ℓ is from -0.9 to 1.1.The resulting optimal values of the variables are shown in the Table 4.2.

Table 4.2. Results of the second level optimization.

	1	2	3	4	5	6	7	8	9	10
r_1	5.018	5.38	4.617	5.306	5.075	6.783	5.019	5.208	2.778	6.194
r_2	2.854	2.486	3.265	3.419	3.998	3.844	4.526	2.245	4.636	5.034
r_3	4.064	3.856	4.105	3.837	3.679	6.605	2.207	1.958	5.96	2.871
r_4	3.441	3.414	2.982	3.717	4.598	3.166	5.156	3.179	5.148	1.102
L_o	14.734	15.362	15.172	15.35	16.2	15.705	16.443	13.742	16.502	17.3
t_b	3.031	2.703	3.288	2.783	1.378	0.908	0.924	2.214	3.425	2.091
H	22.651	21.071	21.951	21.925	20.272	16.584	21.196	22.562	16.958	21.1
ℓ	0.413	0.415	0.35	0.429	0.17	0.355	0.021	-0.07	1.005	0.254
Cost	1.5484	1.5666	1.5278	1.5492	1.4581	1.4156	1.4296	1.4380	1.7611	1.4559

As it can be seen in Table 4.2, the lowest cost is 1.4156 dollars which is obtained in the sixth iteration. For the optimum part, the material cost is 1.4081 dollars, the forging cost is 0.0031894 dollars and the shearing cost is 0.00427893 dollars. Constraints are not violated but lower and upper bounds of dimensions and allowable stress values restricted the part dimensions to avoid penalty terms in objective function. Beside cost terms of optimum I-beam, energy and stress values are given in the Table 4.3.

Table 4.3. Energy and stress values for optimum part.

Strain Energy	$0.381042.10^5$ N.mm
Shearing Energy	$0.10224.10^6$ N.mm
Max. Stress	$0.182932.10^3$ MPa
Max. Contact Pressure	$0.11984.10^4$ MPa
Flash Length	1,60598 mm

The shape of the optimum part, the von Mises stress distribution in the part and equivalent plastic strain in the optimum part are shown in Figure 4.1, Figure 4.2 and Figure 4.3, respectively.

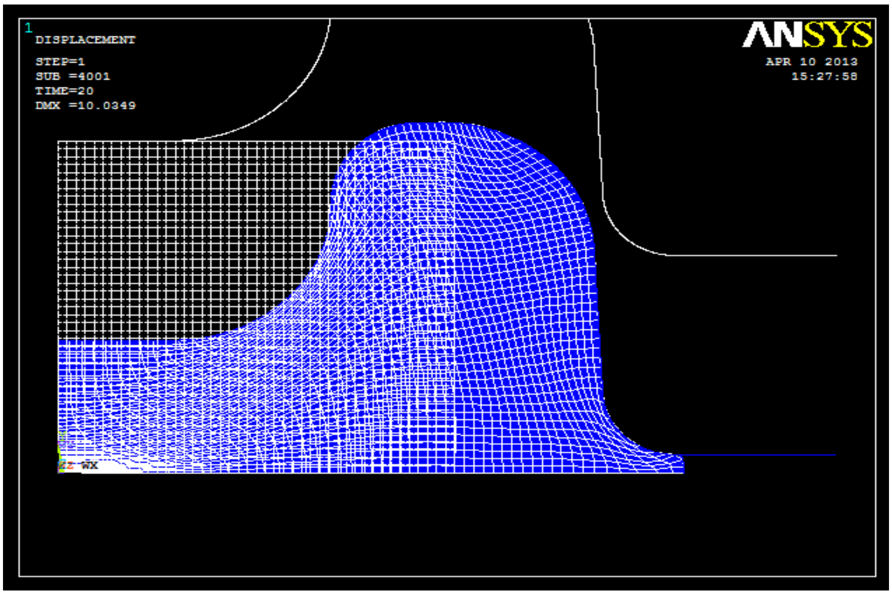

Figure 4.1. The final shape of the optimum part.

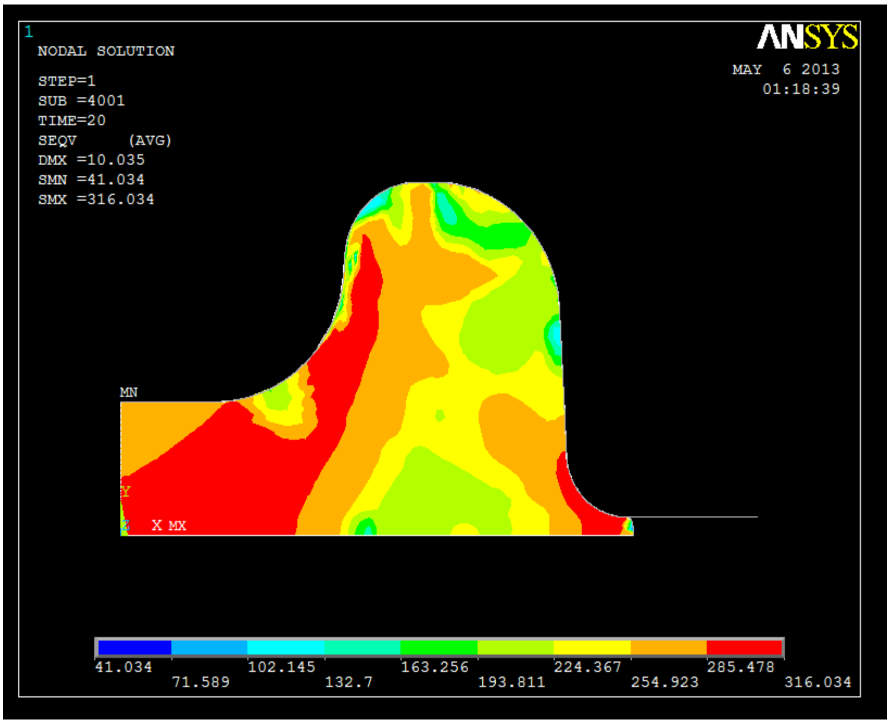

Figure 4.2. Von Mises Stress in the optimum part.

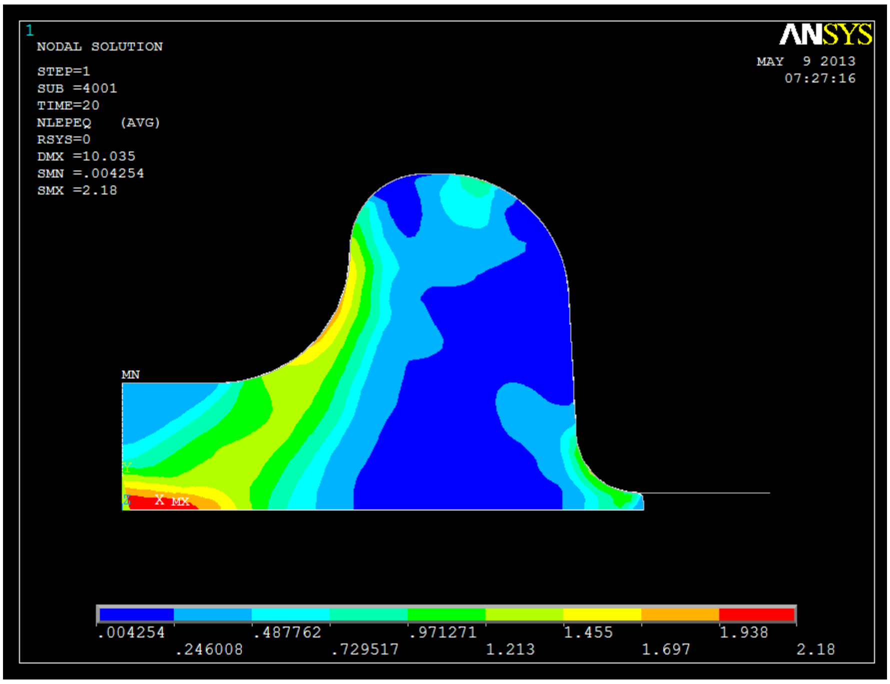

Figure 4.3. Equivalent plastic strain in the optimum part.

5. SUMMARY AND CONCLUSIONS

In this thesis, a concurrent optimization approach is adopted to minimize the total cost of a forged product including material cost, forging cost and post manufacturing (shearing) cost.

There are many studies in the literature on the optimization of forging processes. However, in these studies design variables and design constraints were not considered; therefore a concurrent design approach was not adopted. In this thesis, not only a concurrent approach is adopted in the design optimization procedure, but also a more comprehensive process optimization is conducted.

In this study, an I-beam under a centric load in a simply supported configuration is considered and its cost is minimized using both design and manufacturing parameters as optimization variables. The design variables are the dimensions of the I-beam; the manufacturing variables are the fillet radii, thickness of the flash, and preform dimensions. Both design and manufacturing constraints are applied. The behavioral constraints include failure conditions due to static yielding and local buckling during the use of the beam and the manufacturing constraints include die filling, the maximum allowable pressure on the die and limited flash out of the die.

A multilevel optimization approach is adopted; in the first level, the design of the product is optimized; in the second level, mainly the forging process is optimized. Nelder-Mead, which is a zero-order algorithm, is selected as the search algorithm to find the optimum process and product design. Because, it is a deterministic local search algorithm, the optimization process is repeated many times starting from randomly chosen configurations within the feasible domain in order to obtain the global or near global optimum configuration. Analysis of the cold forging process is performed and the optimization process is conducted in ANSYS.

The proposed concurrent design optimization method proved to be effective. It not only ensured the manufacturability of the designed part, but also optimized the part design as well as the process design. The method developed in this thesis can be applied to the optimization of different forged products. For different parts, only different variables and constraints need to be defined.

APPENDIX A: NELDER MEAD ALGORITHM

The movement of the triangle is achieved by four operations; reflection, expansion, contraction and shrink. Algorithm starts with the calculation of reflection point which requires calculation of middle point. Logic of the algorithm includes comparison of new points with the different points of the triangle. Firstly reflection point function value is compared with good point value and according to this comparison next comparison takes place. Table A.1 shows the all steps of the Nelder-Mead algortithm and comparison between values of the triangle points and new points.

Table A.1. Logical decisions for the Nelder-Mead algorithm [8].

if $f(R) < f(G)$ **then**

perform case(i) {either reflect or extend}

else

perform case(ii) {either contract or shrink}

begin {Case(i)}

if $f(B) < f(R)$ **then**

replace W with R

else

compute E with $f(E)$

if $f(E) < f(B)$ **then**

replace W with E

else

replace W with R

end if

end if

end {Case(i)}

begin {Case(ii)}

if $f(R) < f(W)$ **then**

replace W with R

compute $C = (W + M)/2$

or $C = (M + R)/2$ and $f(C)$

end if

if $f(C) < f(W)$ **then**

replace W with C

else

compute S with $f(S)$

replace W with S

replace G with M

end if

end {Case(i)}

end if

For a function with two variables, formulations of new points are

$$M = \frac{B+G}{2} \tag{A.1}$$

$$R = M + (M - W) = 2M - W \tag{A.2}$$

$$E = R + (R - M) = 2R - M \tag{A.3}$$

where B is best, G is good, W is worst, M is middle, R is reflection and E is expansion point.

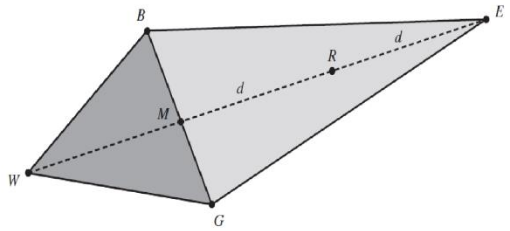

Figure A.1. Triangle *BGW* and point ***R*** and extended point ***E*** [8].

According to the comparion of function values at good and reflection points case *i* or case *ii* is applied.

In the case *i* if the function values at best point worst than reflection point expansion point and function values are calculated as shown in Figure A.1.

In the case *ii*, other points must be tested which are the contradiction points as shown in Figure A.2 and their formulations are

$$C_1 = \frac{M+R}{2} \tag{A.4}$$

$$C_2 = \frac{M+W}{2} \tag{A.5}$$

where C_1 and C_2 are contradiction points.

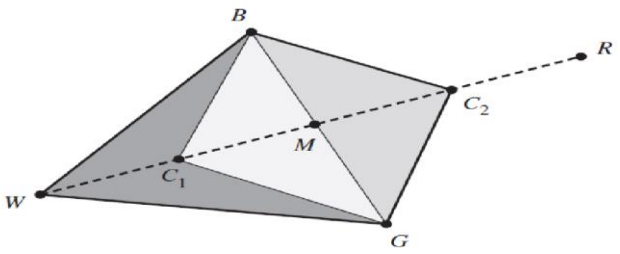

Figure A.2. The contraction point C_1 or C_2 for Nelder-Mead method [8].

If the function value at contradiction pointsis not less than the value at worst point, the points goodand worstmust be shrunk toward best pointas shown in Figure A.3 and formula is

$$S = \frac{B + W}{2} \tag{A.6}$$

where S is shrunk point.

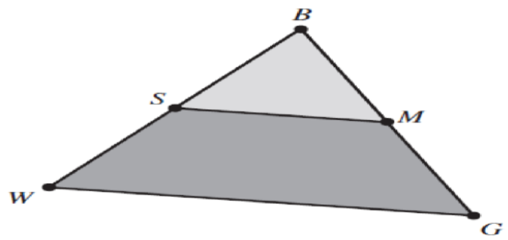

Figure A.3. Shrinking the triangle toward ***B*** [8].

The Nelder-Mead method requires the calculation of the objective function at n+1 initial vertex for n unknowns. Basically, the method is a pattern search that compares function values at vertices. The worst vertex, where the function value becomes largest, is rejected and replaced with a new vertex. A new simplex is formed and the search is continued. The process generates a sequence of simplex for which the function values at the vertices get smaller and smaller. Nelder-Mead algorithm does not require numerical derivatives of the objective function which is the main advantage of this algorithm.

APPENDIX B: FLOW CURVE DATA USED IN MISO MODEL

Table B.1. Flow curve data used in MISO model.

SAE 1010					
Number	Strain	Stress	Number	Strain	Stress
1	0	0	16	0.8	295.1
2	0.001028	216	17	0.9	300.4
3	1140	217	18	1	301.7
4	0.123	232	19	1.25	305.1
5	0.193	248	20	1.5	309.5
6	0.24	260	21	1.75	312.8
7	0.326	276	22	2	315.1
8	0.3387	277	23	2.25	316.4
9	0.3843	278	24	2.5	318.6
10	0.4	278.9	25	2.75	320.8
11	0.45	280.3	26	3	322.0
12	0.5	280.9	27	3.25	324.2
13	0.55	282.6	28	3.5	326.25
14	0.6	285.2	29	3.75	327.6
15	0.7	290.9	30	4	328.2

APPENDIX C: VOLUME OF DIE CAVITY

$$L = V_d / H + \ell \tag{C.1}$$

$$L = \frac{\begin{array}{l} \frac{r_2^{\,2}.\tan\alpha_1}{2} - h.r_2.\tan\alpha_1 - \frac{t_b^{\,2}.\tan\alpha_2}{2} - \frac{\pi.r_1^{\,2}}{4} - L_1.h_s - t_b.\left(r_4.\tan\alpha_2 - r_4\right) - r_1.h_s \\ -r_1^{\,2} + \left(h.h_s.\tan\alpha_1\right) - \left(h_s.r_1.\tan\alpha_1\right) + h.r_2 + h_s.r_2 - r_2^{\,2} - \left(\frac{r_1^{\,2}.\tan\alpha_1}{2}\right) \\ -\left(h_s.r_2.\tan\alpha_1\right) + \frac{\pi.r_2^{\,2}}{4} + h.w + h_s.w - h..r_3 + h_s..r_3 - r_3^{\,2} + \frac{\pi.r_3^{\,2}}{4} \\ +\left(\frac{h^2.\tan\alpha_2}{2}\right) + \frac{H^2.\tan\alpha_2}{2} + \frac{s^2.\tan\alpha_2}{2} + \left(\frac{r_3^{\,2}.\tan\alpha_2}{2}\right) - \frac{r_4^{\,2}.\tan\alpha_2}{2} \\ +h_s.h.\tan\alpha_2 - h.r_3.\tan\alpha_2 - H.s.\tan\alpha_2 + r_4^{\,2} - \frac{\pi.r_4^{\,2}}{4} - \frac{h^2.\tan\alpha_1}{2} \end{array}}{H} + \ell \tag{C.2}$$

APPENDIX D: LATERAL BUCKLING

The critical moment of the I-beam is determined by the energy method. The strain energy U is composed by two parts; energy due to bending about y axis and the enrgy due to twisting about the x axis. Total strain energy is

$$U = \frac{1}{2} E.I_{yy}.\int_0^L \left(\frac{d^2u}{dz^2} \right)^2 dz + \frac{1}{2} G.J.\int_0^L \left(\frac{d\phi}{dz} \right)^2 dz + \frac{1}{2} E.I_w.\int_0^L \left(\frac{d^2\phi}{dz^2} \right)^2 dz \qquad \text{(D.1)}$$

The potential energy of the external loads for a beam subjected to concentrated load P at the middle of the length is

$$W = Pv_w(z) = \frac{P^2}{2.E.I_{yy}} \int_0^L \left(z^2\phi^2 \right) dz \qquad \text{(D.2)}$$

Combining equations total potential energy is obtained as

$$V = U - W \qquad \text{(D.3)}$$

Both ends are simply supported and boundary conditions are applied as following

$$u(0) = u(L) = u^{II}(0) = u^{II}(L) = 0 \qquad \text{(D.4)}$$

$$\phi(0) = \phi(L) = \phi^{II}(0) = \phi^{II}(L) = 0 \qquad \text{(D.5)}$$

Suitable expressions for the buckling form are used in the equations.

$$u(z) = asen\frac{\pi z}{L} \qquad \text{(D.6)}$$

$$\phi(z) = bsen\frac{\pi z}{L} \tag{D.7}$$

Critical load is obtained as

$$P_{cr} = \frac{4\pi^2}{l^2}\sqrt{\frac{3}{\pi^2+6}EI_{yy}\left(GJ+\frac{EC_1\pi^2}{l^2}\right)} \tag{D.8}$$

where E is modulus of elasticity, G is shear modulus of elasticity which, C_1 is torsion warping constant, and J is torsion constant.

$$C_1 = \frac{I_{yy}h_w^{\ 2}}{4} \tag{D.9}$$

$$J = \frac{1}{3}\sum m_i t_i^3 \tag{D.10}$$

For I-beams torsion constant is obtained as follows.

$$J = \frac{2bt_f^{\ 3} + \left(h_w + t_f\right)t_w^{\ 3}}{3} \tag{D.11}$$

Moment of inertia is used in the equation above and calculated as following

$$\begin{aligned}
\mathrm{I}_{YY} &= 2\frac{1}{12}(b-2r_3)^3\, t_f + 4\left\{\frac{1}{3}\left[t_f - r_3 - r_2\right]r_3^{\,3} + \left[t_f - r_3 - r_2\right]r_3\left(\frac{b-2r_3}{2}\right)^2\right\} + \frac{1}{12}h_w t_w^{\ 3} \\
&+4\left\{\frac{\pi}{16}r_3^{\,4} + \frac{\pi r_3^{\,2}}{4}\left(\frac{b}{2} - r_3\right)^2\right\} + 4\left\{\frac{\pi}{16}r_2^{\,4} + \frac{\pi r_2^{\,2}}{4}\left(\frac{b}{2} - r_2\right)^2\right\} \\
&+4\left\{\frac{1}{3}r_1^{\,4} + r_1^{\,2}\left(\frac{t_w}{2} + r_1\right)^2 - \left[\frac{\pi}{16}r_1^{\,4} + \frac{\pi r_1^{\,2}}{4}\left(\frac{t_w}{2} + r_1\right)^2\right]\right\}
\end{aligned} \tag{D.12}$$

APPENDIX E: MAXIMUM DISTORTION ENERGY THEORY

For a given material failure by yielding will occur at a critical level of distortion energy. Therefore distortion energy is computed for a general loading and found by computing the total strain energy and then substracting that due to volumetric change.

Normal stress σ_x acting on a unit cube will cause an extension in its direction

$$\varepsilon_x = \frac{\sigma_x}{E} \tag{E.1}$$

and extension in other directions with Poisson effect

$$\varepsilon_y = \varepsilon_z = -v\frac{\sigma_x}{E} \tag{E.2}$$

Considering unit tube with principal stresses σ_1, σ_2 and σ_3 acting, extensions become

$$\varepsilon_1 = \frac{\sigma_1}{E} - v\frac{\sigma_2}{E} - v\frac{\sigma_3}{E} \tag{E.3}$$

$$\varepsilon_2 = \frac{\sigma_2}{E} - v\frac{\sigma_1}{E} - v\frac{\sigma_3}{E} \tag{E.4}$$

$$\varepsilon_3 = \frac{\sigma_3}{E} - v\frac{\sigma_2}{E} - v\frac{\sigma_1}{E} \tag{E.5}$$

The energy in a unit cube of material subjected to these stresses will be the work done during the application of the stresses. The work done by σ_1 is

$$W_1 = \frac{\sigma_1}{2E}\left(\sigma_1 - v.\sigma_2 - v.\sigma_3\right) \tag{E.6}$$

and similarly for stresses σ_2 and σ_3. Adding the work for three stresses gives

$$W = \frac{\sigma_1}{2E}\left[\sigma_1^{\ 2} + \sigma_2^{\ 2} + \sigma_3^{\ 2} - 2v\left(\sigma_1.\sigma_2 + \sigma_2\sigma_3 + \sigma_3\sigma_1\right)\right] \tag{E.7}$$

This equation includes work due to distortion and due to volumetric changes. Second term is the work which average stress acting in all three directions would do. With all three stresses equal to average stress becomes

$$W_{\Delta Vol} = \frac{1-2v}{6E}\left[\sigma_1^{\ 2} + \sigma_2^{\ 2} + \sigma_3^{\ 2} + 2\sigma_1.\sigma_2 + 2\sigma_2\sigma_3 + 2\sigma_3\sigma_1\right] \tag{E.8}$$

Substracting from the total strain work W distortion energy is obtained as

$$W = \frac{1+v}{6E}\left[\left(\sigma_1 - \sigma_2\right)^2 + \left(\sigma_2 - \sigma_3\right)^2 + \left(\sigma_3 - \sigma_1\right)^2\right] \tag{E.9}$$

This expression for distortion energy is equated to known situation, tension test, at yielding. At that point $\sigma_1 = S_y$ and $\sigma_2 = \sigma_3 = 0$.

$$W_{tens.test} = \frac{\left(1+v\right)2S_y^{\ 2}}{6E} \tag{E.10}$$

Setting the two works equal, criterion for avoiding failure is

$$\sigma_{eff} = \frac{\sqrt{2}}{2}\left[\left(\sigma_1 - \sigma_2\right)^2 + \left(\sigma_2 - \sigma_3\right)^2 + \left(\sigma_3 - \sigma_1\right)^2\right]^{1/2} \leq \frac{S_y}{FS} \tag{E.11}$$

Left side of equation is called the *von Mises* or *effective stress*. Most of cases work is in two dimensions one principal stress is zero. The principal stresses in the loading plane σ_p and σ_q is used in the equation.

$$\sigma_{eff} = \sqrt{\sigma_p^{\ 2} - \sigma_p \sigma_q + \sigma_q^{\ 2}} \leq \frac{S_y}{FS} \tag{E.12}$$

For plane-stress situation, the principal stresses in equation can be written in terms of σ_x, σ_y and τ_{xy}.

$$\sigma_{eff} = \sqrt{\sigma_x^{\ 2} - \sigma_x \sigma_y + \sigma_y^{\ 2} + 3\tau_{xy}^{\ 2}} \leq \frac{S_y}{FS} \tag{E.13}$$

If there is only one tension stress σ_x and shear stress τ_{xy} as in bending with twisting equations become

$$\sigma_{eff} = \sqrt{\sigma_x^{\ 2} + 3\tau_{xy}^{\ 2}} \leq \frac{S_y}{FS} \tag{E.14}$$

Shear stress is calculated as

$$\tau = \frac{VQ}{I_{zz} t} \tag{E.15}$$

$$\tau = \frac{V.b.t_f \left(h_w + t_f\right)/2}{I_{zz} t_w} \tag{E.16}$$

and equivalent stress becomes

$$\sigma_{eq} = \sqrt{\left(\frac{\frac{WL_b}{4} \cdot \frac{h_w}{2}}{I_{zz}}\right)^2 + 3.\left(\frac{F.b.t_f \left(h_w + t_f\right)/4}{I_{zz} t_w}\right)^2} \tag{E.17}$$

REFERENCES

1. Altan, T., G. Ngaile, G. Shen, “Cold and Hot Forging”, *Fundamentals and Applications, ASM International*, Ohio, 2005.

2. Poursina M., J. Parvizian, C.A.C. Antonio, “Optimum Pre-form Dies in Two-Stage Forging”, *Journal of Materials Processing Technology*, Vol. 174, No. 1–3, pp. 325-333, 2006.

3. Lu B., H. Ou, H. Long, “Die Shape Optimisation for Net-Shape Accuracy in Metal Forming Using Direct Search and Localised Response Surface Methods”, *Structural and Multidisciplinary Optimization*, Vol. 44, No. 4, pp. 529-545, 2011.

4. António C. A C., C. F. Castro, L. C. Sousa, “Optimization of Metal Forming Processes”, *Computers and Structures*, Vol. 82, pp. 1425–1433, 2004.

5. Fourment, L., J. L. Chenot, “Optimal Design for Non-steady-state Metal Forming Processes-I. Shape Optimization Method”, *International Journal for Numerical Methods in Engineering*, Vol. 39, pp. 33-50, 1996.

6. Tumer, H., F. Ö. Sönmez, *Optimum Preform And Die Shape Design For Improved Hardness Distribution In Cold Forged Parts*, M.S. Thesis, Bogazici University, 2007.

7. Zhao G., E. Wright, R. V. Grandhi, “Preform Die Shape Design in Metal Forming Using an Optimization Method”, *International Journal for Numerical Methods in Engineering*, Vol. 40, pp. 1213-1230, 1997.

8. Castro C. F., L.C. Sousa, C.A.C. António, J.M.A. César de Sá, “An Efficient Algorithm to Estimate Optimal Preform Die Shape Parameters in Forging”, *Engineering Computations*, Vol. 18, pp. 1057-1077, 2001.

9. Srikanth A., N. Zabaras, “Shape Optimization and Preform Design in Metal Forming Processes”, *Computer Methods in Applied Mechanics and Engineering*, Vol. 190, No. 13-14, pp. 1859-901, 2000.

10. Shim H., “Optimal Preform Design for the Free Forging of 3D Shapes by the Sensitivity Method”, *Journal of Materials Processing Technology*, Vol. 134, No. 1, pp. 99-107, 2003.

11. Valente R. A. F., A. Andrade-Compos, J. F. Carvalho, P.S. Cruz, “Parameter Identification and Shape Optimization: An Integrated Methodology in Metal Forming and Structural Applications”, *Optimization and Engineering*, Vol. 12, pp. 129-152, 2011.

12. António C. A. C, N. M. Dourado,“Metal-forming Process Optimization by Inverse Evolutionary Search”, *Journal of Materials Processing Technology*, Vol. 121, No. 2-3, pp. 403-413, 2002.

13. Castro C.F., C.A.C. António, L.C. Sousa ,“Optimisation of Shape and Process Parameters in Metal Forging Using Genetic Algorithms”, *Journal of Materials Processing Technology*, Vol. 146, No. 3, pp. 356-364, 2004.

14. António C. C., C. F. Castro, L. C. Sousa, “Eliminating forging defects using genetic algorithms”, *Materials and Manufacturing Processes*, Vol. 20, pp. 509-522, 2005.

15. Chung, J.S., S.M. Hwang,“Process Optimal Design in Forging by Genetic Algorithm”, *Journal of Manufacturing Science and Engineering*, Vol. 124, 2002.

16. Biglari F. R., N. P. O’Dowd, R. T. Fenner, “Optimum Design of Forging Dies Using the Finite Element Method”, *5th ACME-UK Conference, Imperial College, London*, pp.100-104, 1997.

17. Zhao G., E. Wright, R. V. Grandhi, "Sensitivity Analysis Based Preform Die Shape Design for Net-shape Forging", *International Journal of Machine Tools and Manufacture*, Vol. 37, No. 9, pp. 1251-1271, 1997.

18. Cheng H., R.V.Grandhi, "Design of Optimal Process Parameters for Non-isothermal Forging", *International Journal for Numerical Methods in Engineering*, Vol. 37, No. 1, pp. 155-177, 1994.

19. Repalle J., R. V. Grandhi, "Reliability-based Preform Shape Design in Forging" *Communications in Numerical Methods in Engineering*, Vol. 21, No. 11, pp. 607-17, 2005.

20. Khoury, I., L. Giraud-Moreau, P. Lafon, C. Labergere, "Towards an Optimization of Forging Processes Using Geometric Parameters", *Journal of Materials Processing Technology*, Vol. 177, No. 1-3, 2006.

21. Gao Z., R.V.Grandhi, "Microstructure Optimization in Design of Forging Processes", *International Journal of Machine Tools and Manufacture*, Vol. 40, No. 5, pp. 691-711, 2000.

22. Repalle J., R. V. Grandhi, "Design of Forging Process Variables under Uncertainties", *Journal of Materials Engineering and Performance*, Vol. 14, No. 1, pp. 123-131, 2005.

23. Zhao G.Q., R. Huff, A. Hutter, and R.V. Grandhi, "Sensitivity Analysis Based Preform Die Shape Design Using the Finite Element Method", *Journal of Materials Engineering and Performance,* Vol. 6, pp. 303-310, 1997.

24. Zhao X., G. Zhao, G. Wang, T. Wang, "Preform Die Shape Design for Uniformity of Deformation in Forging Based on Preform Sensitivity Analysis", *Journal of Materials Processing Technology,* Vol. 128, pp. 25–32, 2002.

25. Zhao, G., X. Ma, X. Zhao, R. V. Grandhi, “Studies on Optimization of Metal Forming Processes Using Sensitivity Analysis Methods”, *Journal of Materials Processing Technology*, Vol. 147, No. 2, pp. 217-228, 2004.

26. Esche, S. K., C. Chassapis, S. Manoochehri, “Concurrent Product and Process Design in Hot Forging”, *Concurrent Engineering: Research and Applications*, Vol. 9, 2001.

27. Ou H., J. Lan, C.G. Armstrong, M.A. Price, “An FE Simulation and Optimisation Approach for the Forging of Aeroengine Components”, *Journal of Materials Processing Technology*, Vol. 151, No. 1–3, pp. 208-216, 2004.

28. Lu B., H. Ou, C.G. Armstrong, A. Rennie, “3D Die Shape Optimisation for Net-shape Forging of Aerofoil Blades”, *Materials & Design*, Vol. 30, No. 7, pp. 2490-2500, 2009.

29. Lu B., H. Ou, “Stochastic Finite–Element Modelling and Optimization For Net-Shape Forging of Three-Dimensional Aero-Engine Blades”, *Proceedings of the Institution of Mechanical Engineers*, Vol. 225, pp.71-85, 2011.

30. Lu B., H. Ou, S. Cui, “Shape Optimization of Preform Design for Precision Close-die Forging”, *Structural and Multidisciplinary Optimization*, Vol. 44, pp.785–796, 2011.

31. Jolgaf, M., A.M.S. Hamouda, S. Sulaiman, M.M. Hamdan, “Development of a CAD/CAM System for the Closed-die Forging Process”, *Journal of Materials Processing Technology*, Vol.138, 2003.

32. Roy S., S. Ghosh, R. Shivpuri , “A New Approach to Optimal Design of Multi-stage Metal Forming Processes with Micro Genetic Algorithms”, *International Journal of Machine Tools and Manufacture*, Vol. 37, pp. 29-44, 1997.

33. Kim D. H., D. J: Kim, B. M. Kim, “The Application of Neural Networks and Statistical Methods to Process Design in Metal Forming Processes”, *International Journal of Advanced Manufacturing Technology*, Vol. 15, pp. 886–894, 1999.

34. Duggirala R., R. Shivpuri, S. Kini, S. Ghosh, S. Roy, “Computer Aided Approach for Design and Optimization of Cold Forging Sequences for Automotive Parts”, *Journal of Materials Processing Technology*, Vol. 46, pp. 185-198, 1994.

35. Kim D. J., B. M. Kim, J. C. Choi, “Determination of the Initial Billet Geometry for a Forged Product Using Neural Networks”, *Journal of Materials Processing Technology*, Vol. 72, pp. 86-93, 1997.

36. Yanhui Y., L. Dong, H. Ziyan, L. Zijian, “Optimization of Preform Shapes by RSM and FEM to Improve Deformation Homogeneity in Aerospace Forgings”, *Chinese Journal of Aeronautics*, Vol. 23, pp. 260-267, 2010.

37. Vieilledent D., L. Fourment, “Shape Optimization of Axisymmetric Preform Tools in Forging Using a Direct Differentiation Method”, *International Journal for Numerical Methods in Engineering*, Vol. 52, pp. 1301-1321, 2001.

38. Meng, F., C. Labergere, P. Lafon, “Methodology of the Shape Optimization of Forging Dies”, *International Journal of Material Forming*, Vol. 3, pp. 927-930, 2010.

39. Sedighi M., S. Tokmechi, “A New Approach to Preform Design in Forging Process of Complex Parts”, *Journal of Materials Processing Technology*, Vol. 197, No. 1-3, pp. 314-24, 2008.

40. Grandhi R. V., N. Thiyagarajan, “Multi-level Design Process for 3-D Preform Shape Optimization in Metal Forming”, *Journal of Materials Processing Technology*, Vol. 170, No. 1-2, pp. 421-429, 2005.

41. Khaleed, H. M. T., Z. Samad, A. R. Othman, M. A. Mujeebu, A. B. Abdullah, N. J. S. Ahmed, M. M. Zihad, “Flash-less Cold Forging and Temperature Distribution in Forged Autonomous Underwater Vehicle Hubs Using FEM Analysis and Experimental Validation”, *International Journal of Mechanical and Materials Engineering (IJMME)*, Vol. 6, No. 2, pp. 291-29, 2011.

42. Thiyagarajan N., R. V. Grandhi, “3D Preform Shape Optimization in Forging Using Reduced Basis Techniques”, *Engineering Optimization*, Vol. 37, No. 8, pp. 797–811, 2005.

43. Bonte, M. H. A., L. Fourment, T. Do, A. H. Boogaard, J. Huetink, “Optimization of Forging Processes Using Finite Element Simulations: A Comparison of Sequential Approximate Optimization and Other Algorithms”, *Structural and Multidisciplinary Optimization*, Vol. 42, No. 5, pp 797-810, 2010.

44. Poursina M., C.A.C. Antonio, C.F. Castro, J. Parvizian, L.C. Sousa, “Preform Optimal Design in Metal Forging Using Genetic Algorithms”, *Engineering Computation*, Vol. 21, pp. 631-650, 2004.

45. Janakiraman,V., R. Saravanan, ”Concurrent Optimization of Machining Process Parameters and Tolerance Allocation”, *International Journal of Advanced Manufacturing Technology*, Vol. 51, No. 1-4, pp. 357-369, 2010.

46. Khaleed H.M.T., Z. Samad, A.R. Othman, M. A. Mujeebu, A.B. Abdullah, M.M. Zihad, "Work-piece Optimization and Thermal Analysis for Flash-less Cold Forging of AUV Propeller Hubs - FEM Simulation and Experiment", *Journal of Manufacturing Processes,* Vol. 13, pp. 41-49, 2011.

47. Chenot J., E. Massoni, L. Fourment, "Inverse Problems in Finite element Simulation of Metal Forming Processes", *Engineering Computations,* Vol. 13, No. 2-4, pp. 190-225, 1996.

48. Chen X., R. Balendra, Y. Qin, “A New Approach for the Optimization of the Shrink-fitting of Cold-forging Dies*”, Journal of Materials Processing Technology*, Vol. 145, pp. 215-223, 2004.

49. Bonte M. H. A., Boogard A. H., Heutink J, “An Optimization Strategy for Industrial Metal Forming Processes: Modelling, Screening and Solving of Optimisation Problems in Metal Forming”, *Structural and Multidisciplinary Optimization*, Vol. 35, No. 6, pp 571-86, 2008.

50. Chang K., I. H. Bryant “Concurrent Design and Manufacturing of Aircraft Torque Tubes”, *Journal of Materials Processing Technology*, Vol., 150, pp. 151-162, 2004.

51. Al-Ansary M.D., I.M. Deiab, “Concurrent Optimization of Design and Machining Tolerances Using the Genetic Algorithms Method”, *International Journal of Machine Tools and Manufacture*, Vol. 37, pp. 1721-1731, 1997.

52. Chen L., L. Simon, “A Computerized Team Approach for Concurrent Product and Process Design Optimization”, *CAD Computer Aided Design*, Vol. 34, pp. 57-69, 2002.

53. Öztürk M., F. Ö. Sönmez, *Optimization of Forging Processes with a Concurrent Approach*, M.S. Thesis, Boğaziçi University, 2008.

54. Öztürk M., F. Ö. Sönmez, “Optimization of Forging Processes with a Concurrent Approach”, *5 th International Conference on Design and Production of Machines and Dies/Mold*, 2009.

55. Andrade A., D. Camotim, P. Providencia e Costa., "On the Evaluation of Elastic Critical Moments in Doubly and Singly Symmetric I-section Cantilevers", *Journal of Constructional Steel Research*, Vol. 63, pp. 894-908, 2007.

56. Megson, T. H. G., *Structural and Stress Analysis*, Butterworth-Heinemann, 2000.

57. Sanchez H.A., Cortes C., *Lateral buckling of steel I-beams with different boundary conditions by numerical simulation, Behaviour of steel structures in Seismic Areas*, STESSA, 2012.

58. Material Property Data, “Properties of SAE 1010”, 1996, http://www.matweb.com/search/DataSheet.aspx?MatGUID=025d4a04c2c640c9b0eaaef 28318d761&ckck=1, August 2011.

59. Schey J. A., *Introduction to Manufacturing Processes*, Third Edition, McGraw-Hill Book Company, Boston 1999.

60. Byon, S. M., S.M. Hwang, “Process Optimal Design in Non-isothermal, Steady-state Metal Forming by the Finite Element Method”, *International Journal of Mechanical Sciences*, Vol.42, No. 5, pp. 965-990, 2000.

61. Kovrizhnykh A. M., “Determining Shear Angle, Forces, and Sizes of Shearing Elements During Metal Cutting”, *Journal of Applied Mechanics and Technical Physics,* Vol. 50, No. 1, pp. 147-154, 2009.

62. ICDAS, “Current Price List”, 2010, http://www.icdas.com.tr/icdas/yurtici_ fiyat_tr.htm, May 2012.

63. Energy Institute, “Electricity price list of 2011”, 2011 http://enerjienstitusu. com/2011/01/11/2011-yili-yeni-elektrik-tarifesi/#more-427, May 2011.

64. Doltsiniz I., T. Rodic, “Process Design and Sensitivity Analysis in Metal Forming”, *International Journal for Numerical Methods in Engineering*, Vol. 45, pp. 661- 692, 1999.

65. Ansys, “Release 12.1 Documentation”, ANSYS Inc., 2011.

66. Boller C., T. Seeger, *Materials Data for Cyclic Loading Part A: Unalloyed Steels,* Amsterdam ; New York : Elsevier, 1987.